学　位　論　文

Studies about a therapeutic efficacy of EVA1-Antibody Drug Conjugate using glioblastoma-bearing mouse model
(膠芽腫モデルマウスを用いた EVA1−抗体薬物複合体の治療効果に関する研究)

2025 年 3 月

北　海　道　大　学
侯　佳　慧

学　位　論　文

Studies about a therapeutic efficacy of EVA1-Antibody Drug Conjugate using glioblastoma-bearing mouse model
(膠芽腫モデルマウスを用いた EVA1−抗体薬物複合体の治療効果に関する研究)

2025 年 3 月

北　海　道　大　学
侯　佳　慧

Contents

List of publications and presentations

List of Publications

1. Hou, J., Uejima, T., Tanaka, M., Son, Y.L., Hanada, K., Kukimoto-Niino, M., Yamaguchi, S., Hashimoto, S., Yokoyama, S., Takemori, T., Saito, T., Shirouzu, M., Kondo, T. EVA1-Antibody Drug Conjugate is a new therapeutic strategy for eliminating glioblastoma-initiating cells. Neuro-Oncology, noae226 (2024).

List of Presentations

1. Hou, J., Kondo, T. Eva1 antibody: a novel therapeutic antibody for glioblastoma. The 42nd Sapporo international Cancer Symposium, Jun6-8, 2024, Mercure Sapporo Odori Park, Sapporo, Japan.

Summary

Background and Purpose:

Glioblastoma (GBM) represents a highly aggressive and prevalent form of brain cancer. Although it has been thought that GBM originates from astrocytes, there are many evidence showing that neural stem cells (NSCs) and oligodendrocyte precursor cells (OPCs) are alternative cell-of-origin of GBM (Noble et al, 1995; Hide et al, 2011). The standard treatment for GBM is a combination of surgery, radiation, and chemotherapy. Despite of the extensive efforts, a median survival period, approximately 15 months, has not been changed (Stupp et al, 2005; Stupp et al, 2009). The identification of GBM-initiating cells (GICs) has redirected the focus of GBM research (Kondo, 2006; Singh et al, 2004; Vescovi, 2006). GICs have been demonstrated to be tumorigenic and be resistance to radiation and chemotherapy, suggesting that it is the cell-of-origin for the recurrence. Therefore, it is crucial to characterize GIC and identify the targets that are either specific or essential for the cells. Comparing the expression profiles of GICs and their potential cell-of-origins, NSCs and OPCs, we have shown that Epithelial V-like antigen 1 (EVA1) is a novel and functionally specific factor in GICs (Ohtsu et al, 2016).

EVA1 has been originally identified as a factor involved in T cell development in thymus (Guttinger et al, 1998). EVA1 is a type-1 transmembrane protein with a V-like structure in the extracellular domain, suggesting that EVA1 is involved in the cell-cell adhesion. However, it is yet unknown about its physiological function, except in our previous finding that EVA1 plays an essential role in GICs by activating non-canonical NF-κB signaling pathway (Ohtsu et al, 2016). Moreover, we found that EVA1 is upregulated in GBM and is associated with worse prognosis in patients with other cancers, such as breast cancer and pancreatic cancer, using public databases. Taken together, we started to develop a new antibody drug targeting EVA1 for GBM therapy.

Subjects and Methods:

Hybridoma cells were initially generated through the immunization of BALB/c mice with the EVA1-Fc fusion protein. Subsequently, the reactivity of the supernatant derived from these hybridoma cells was meticulously examined using EVA1-overexpressing cells and GICs. Candidate antibodies were then further screened using Biacore surface plasmon resonance analysis with antibody-dependent cellular cytotoxicity (ADCC) and complement-dependent cytotoxicity (CDC). Among

candidate antibodies, B2E5 was selected. To achieve large-scale production of the B2E5 antibody, the hybridoma cells were injected into the abdominal cavity of NOD/SCID mice. The ascites fluid that had been generated was harvested, and following a purification process, the B2E5 monoclonal antibody was successfully obtained. To identify the epitope of B2E5, we generated a set of mutant EVA1, examined their binding with B2E5. To explore the therapeutic potential of B2E5 as a therapeutic antibody for GBM, IgG-ADC and B2E5-ADC were generated by conjugating mouse IgG and B2E5, respectively, with a potent mitotic inhibitor, MMAE (Monomethyl Auristatin E). The cytotoxicity of the B2E5-ADC was comprehensively evaluated by both adding it to cultured GICs and intracranially injecting it into GIC tumor-bearing brains.

Results:

I selected B2E5, as a potential candidate of the antibody drug, by its high affinity to EVA1 and the cytotoxic activities, ADCC and CDC. I determined P72 as the epitope of B2E5, by the binding assay with a set of mutant EVA1. I found that B2E5 was internalized into GICs over time and demonstrated that B2E5 conjugated with MMAE (B2E5-ADC) effectively killed GIC with its concentration-dependent manner in vitro. I established two Enhanced Luciferase-expressing GIC lines (ELuc-GICs, ELuc-E6 and ELuc-E16). Using a GBM-bearing mouse model that was transplanted with ELuc-GICs, I demonstrated that intracranial injection of B2E5-ADC effectively eliminated GICs with their death and the invasion of microglia/macrophages and significantly extended the survival time of the mice.

Discussion:

I successfully demonstrated that intracranial injection of B2E5-ADC killed GICs in brains of tumor-bearing mice and significantly extended their survival time. Considering the clinical setting, however, the intracranial injection is highly invasive and difficult to inject B2E5-ADC multiple times to the patients. Therefore, developing an effective and non-invasive method delivering B2E5-ADC into brain is crucial for the therapy. Alternatively, we may use smaller antibody-based molecules, such as Fab (fragment of antigen-binding)-ADC and scFv (single-chain fragment variable)-ADC, which can more easily traverse the blood-brain barrier (BBB).

In this study, I observed that B2E5-ADC extended the lifespan of GIC-bearing mice yet failed to achieve a complete cure as all mice succumbed 60 days post-tumor

transplantation. Two potential reasons underlie this. Firstly, residual GIC tumors in the brain led to recurrence upon cessation of B2E5-ADC treatment, resulting in the mice's demise. To address this, we could consider increasing either the concentration or frequency of B2E5-ADC administration to ensure complete tumor elimination. Secondly, the severe and irreversible brain tissue damage caused by GBM is a contributing factor. Brain tumors can precipitate a host of serious consequences, including neurological dysfunction, cognitive impairment, epilepsy, elevated intracranial pressure, and associated complications.

I observed hemosiderin deposition in the brain that had been injected with B2E5-ADC, whereas no such deposition was observed in the brains injected with either IgG, B2E5, or IgG-ADC. This finding implies that the hemosiderin deposits likely originated from dead GBM cells (GICs), given that previous studies have demonstrated that GBM cells overexpress transferrin receptor and consequently accumulate iron within the cells. (Recht et al, 1990; Voth et al, 2015). Another possible explanation is that microglia or macrophages scavenged apoptotic GICs, which subsequently led to the formation of hemosiderin deposits. In either of these two scenarios, the occurrence of hemosiderin deposits presumably serves as an indicator or a characteristic feature of the elimination of GICs mediated by B2E5-ADC.

I demonstrated that the intracranial injection of B2E5-ADC was highly effective in impeding brain tumorigenesis in the E6 and E16 models. For clinical translation and application, it will be necessary in the future to conduct further evaluations regarding the efficacy of B2E5-ADC in other well-established brain tumor models.

Conclusion:

Our data indicate that B2E5-ADC is a new and promising therapeutic strategy for GBM.

List of Abbreviations

AA: anaplastic astrocytoma

AAs: amino acids

Ab: antibody

ADC: antibody-drug conjugate

ADCC: antibody-dependent cellular cytotoxicity

AE: anaplastic ependymoma

AO: anaplastic oligodendroglioma

AS: ascites

BALB/c: Bagg's Albino c/c

BBB: blood-brain-barrier

BSA: bovine serum albumin

bFGF: basic fibroblast growth factor

Casp3: caspase 3

CC50: half maximal cytotoxic concentration

CDC: complement-dependent cytotoxicity

Daudi-EVA1: epithelial v-like antigen 1-overexpressing daudi cells

DMEM: dulbecco's modified eagle medium

DMG: diffuse midline glioma

DMSO: dimethyl sulfoxide

DNA: deoxyribonucleic acid

DTT: dithiothreitol

EGF: epidermal growth factor

ELuc-GICs: enhanced luciferase-expressing glioblastoma-initiating cells

EVA1: epithelial v-like antigen 1

Fab-ADC: fragment of antigen-binding antibody-drug conjugate

FBS: fetal bovine serum

GBM: glioblastoma

GG: ganglioglioma

GICs: glioblastoma-initiating cells

HAT medium: hypoxanthine aminopterin thymidine medium

H&E staining: hematoxylin and eosin staining

hGICs: human glioblastoma-initiating cells

HPA: Human Protein Atlas

ICC: immunocytochemistry

Ka: association rate constant

Kd: dissociation rate constant

K_D: dissociation equilibrium constant

MMAE: monomethyl auristatin e

MTT: 3-(4,5-Dimethyl-2-thiazolyl)-2,5-diphenyl-2H-tetrazolium bromide

na: not available

NOD/SCID: non-obese diabetic/severe combined immunodeficiency

ns: not significant

NSC: neural stem cell

OPCs: oligodendrocyte precursor cells

PA: pilocytic astrocytoma

PBS: phosphate-buffered Saline

PCR: polymerase chain reaction

PEI: polyethyleneimine

PFA: paraformaldehyde

qPCR: quantitative polymerase chain reaction

RNA: ribonucleic acid

RT-PCR: reverse transcription polymerase chain reaction

RTX: rituximab

SD: standard deviation

scFv-ADC: single-chain fragment variable antibody-drug conjugate

TMZ: temozolomide

WHO: world health organization

Introduction

Gliomas are brain tumors possessing the characteristics of glial cells, mainly astrocytes and oligodendrocytes, and have been classified into four grades (WHO grade I–IV) based on their pathologic features. Glioblastoma (GBM) is one of most malignant gliomas (WHO grade IV), and a devastating brain cancer resulting in death within 6 months, if untreated. Patients with GBM have a median survival of approximately 15 months (Stupp et al, 2005; Stupp et al, 2009). Despite tremendous efforts to effectively treat GBM, the overall survival rates of GBM patients have remained unchanged over the past few decades. GBM has unique treatment challenges due to 1) tumor is localized in the brain and malignant cells invade adjacent brain tissue, thus it is difficult to be surgically removed; 2) GBM has inherent resistance to conventional therapy, such as adjuvant temozolomide (TMZ) chemotherapy and radiotherapy. Since there are few effective treatment strategies for GBM, the development of new drugs is particularly urgent and important.

GBM-initiating cells (GICs) are a subset of cancer cells with strong self-renewal and invasion abilities, playing an important role in tumorigenesis and metastasis and expresses stem cell markers such as CD133 (also known as Prominin1), Sox2, CD15 (also known as Stage-Specific Embryonic Antigen 1 and Lewis X), and cd49f (also known as integrin α 6). In addition, GICs tends to survive after therapeutic approaches (such as radiotherapy and chemotherapy), thus leading to treatment failure and tumor recurrence. Thus, GIC-targeting approaches could be a breakthrough for cancer therapy.

Previously, we generated mouse GIC lines, NSCL61 and OPCL61 (Hide et al, 2009; Hide et al, 2011). This was achieved by overexpressing the oncogenic HRasL61 in p53-deficient neural stem cells (NSCs) and oligodendrocyte precursor cells (OPCs) respectively. These mouse GICs exhibited the capacity to form transplantable GBMs, displaying characteristics such as hypercellularity, pleomorphism, multinuclear giant cells, mitosis, and necrosis. Notably, even with a minimal injection of only ten cells into the brains of nude mice, the formation of GBMs could be observed. Additionally, we established human GICs, including E6 and E16, which were derived from independent GBM specimens (Takezaki et al, 2011; Yamashita et al, 2015). These hGICs were capable of forming GBM-like brain tumors when transplanted into the brains of immunodeficient mice. To identify novel GIC factors, we compared gene expression profiles of mouse and human GICs with those of their cells-of-origin,

NSCs and OPCs, and eventually focused on Epithelial V-like antigen 1 (EVA1, also known as Myelin protein zero like 2) as a potential candidate.

EVA1 was initially recognized as a member of the immunoglobulin superfamily that is expressed on the cell-surface membrane of developing thymus epithelial cells and vanishes in the developed stage. In our prior research, EVA1 was identified as a novel and functionally specific factor in GICs (Ohtsu et al, 2016); EVA1 is highly expressed in both human and mouse GICs but not in either non-tumorigenic GBM cells or normal neural stem cells. The knockdown of *Eva1* in GICs led to a reduction in their self-renewal and tumorigenic capabilities, while Eva1 overexpression enhanced tumorigenicity in low-grade glioma. Together with an evidence that Eva1 expression is low in mouse tissues, we started to generate anti-EVA1 antibodies with high affinity.

Herein, we present that B2E5, one of EVA1 Abs is a potential candidate antibody for GBM treatment. B2E5 bound to human EVA1 with high affinity and eliminated EVA1-expressing cells in culture by ADCC and CDC. We demonstrated that B2E5-monomethyl auristatin e (MMAE) conjugate (B2E5-ADC) effectively killed GICs in culture and prevented GIC tumorigenesis in brain of nude mice when injected intracranially. Together, these data indicated that B2E5 can serve as a novel therapeutic antibody against GBM.

Materials and Methods

Animals and chemical reagents

All experiments involving mice were conducted in according to protocols approved by the Animal Care and Use Committees of Hokkaido University and the RIKEN Animal Care and Use Committee. BALB/c and KSN/Slc nude mice were obtained from CLEA Japan and Sankyo Lab Service Corporation Japan (SLC Japan), respectively. Chemicals and growth factors were purchased from Invitrogen, Sigma and PeproTech, unless otherwise indicated.

Glioblastoma-initiating cell culture and cell lines

E6 and E16 hGICs were established by culturing dispersed human GBM tissues in a half-medium containing a 1:1 mixture of neural stem cell (NSC) medium and DMEM (Nacalai, 08458-16) with fetal bovine serum (FBS; 10%, BioWest, S1580), penicillin streptomycin (Gibco). NSC medium consists of DMEM/F12 (Sigma, D8062) with bovine insulin (10 μg/ml, Sigma, I6634), human transferrin (100 μg/ml, Sigma, T1147), BSA (100 μg/ml, Sigma, A4161), progesterone (60 ng/ml, Sigma, P878), putrescine (16 μg/ml, Sigma, P7505), sodium selenite (40 ng/ml, Sigma, S5261), N-acetylcysteine (60 μg/ml, Nacalai Tesque), forskolin (5 μM, Sigma, F6886), sodium pyruvate (Nacalai Tesque, 08458-16), d-biotin (10 ng/ml, Nacalai Tesque, 04822-91), Glutamax (1%, Gibco, 35050), human bFGF (20 ng/ml), human EGF (20 ng/ml), penicillin streptomycin (Gibco). Each GIC line were confirmed to maintain GIC characteristics, including self-renewal, NSC marker expression, sphere formation and tumorigenicity, in the half-medium. ELuc-GICs were generated by infecting cells with the pLV CEH iRFP670-ELuc IB vector (a gift from Dr. Yasuhito Onodera). PLAT-A, HEK293F and 293T cells were maintained in DMEM supplemented with 10% FCS. Eluc-GICs were cultured in NSC half medium with Blasticidin S (10 ng/ml, Wako).

For MTT assay, cells were cultured on 96-well plates (WATSON); the hGICs were cultured in half-medium.

For ICC, hGICs were cultured on poly-D-lysine (15 mg/mL, Sigma)-coated cover slides in 4-well plate (Thermo Scientific™ Nunc™ IVF)

Vector

Human *EVA1* (*EVA1*) cDNA was purchased from OriGene. To construct expression vectors for human *EVA1* and mouse *Eva1*, their full-length cDNAs were inserted into

the pMY-IRES-EGFP retrovirus vector (a gift from Dr. Toshio Kitamura), resulting in pMY-EVA1-IRES-EGFP and pMY-Eva1-IRES-EGFP, respectively.

Mutant *EVA1* cDNAs were constructed using the PrimeSTAR® Mutagenesis Basal Kit (TAKARA-BIO), with mutagenic fragments assembled by In-Fusion (TAKARA-BIO) and subsequently inserted into pMY-IRES-EGFP vectors. All introduced mutations were verified by DNA sequencing.

Generation of Mouse Anti-EVA1 Monoclonal Abs

To generate the EVA1-Fc protein as an antigen, pINFUSE-EVA1-mIgG2bFc1 was transfected into HEK293F cells. The supernatant was used to purify EVA1-Fc. Ninety-six hours after transfection, the supernatant (1 liter) was harvested and applied to an rProteinA-sepharose column (Cytiva). After washing the column with a 20mM Tris-HCl (pH7.5, Nacalai) and 0.3M NaCl buffer, EVA1-Fc was eluted with a 100 mM arginine solution (pH 3.5), quickly neutralized by adding Tris-HCl (pH 9.0, 1 M) to a final concentration of 0.25 M. The protein was concentrated using an Amicon Ultra Centrifugal Filter (Merck Millipore) and then fractionated on a HiLoad Superdex200 column (Cytiva) equilibrated with 20 mM Tris-HCl (pH 8.0), 150 mM NaCl, and 2 mM DTT.

Hybridoma cells were generated as follows: BALB/c mice were immunized with purified EVA1-Fc along with Titer Max Gold adjuvant (Sigma Aldrich, St. Louis, MO) in their foot pads, followed by a booster with the same antigen two weeks later. Three days after boosting, lymphoid cells from the draining lymph nodes were purified and fused with the P3U1 cell line using polyethylene glycol. The fused cells were cultured in a 96-well flat-bottom plate and selected in HAT medium (sodium hypoxanthine, aminopterin and thymidine).

B2E5 antibody generation

During EVA1 antibody initial selection, I generated antibodies from hybridoma cell supernatant. After identifying B2E5 as a suitable candidate, I changed to ascites method for B2E5 antibody production. Hybridoma cells (10^7 cells/mice) were intraperitoneally injected into the abdominal cavity of immunodeficient NOD/SCID mice. Following a waiting duration of one to two weeks, the generated ascites fluid was collected. Subsequently, the obtained ascites fluid was purified using NAb™ Protein A Plus Spin Kits (Thermo Scientific, 89978). Then, the B2E5 antibody was

concentrated, and the solvent was replaced with PBS using the centrifugal concentrator (Vivaspin turbo 15).

B2E5 antibody purification

Protein G resin column (Protein G Sepharose 4 fast flow, Cytiva) was used to purify antibodies. Equilibrate the column and buffers to room temperature. Remove storage solution and dilute the sample 1:1 with binding buffer (100mM phosphate, 150mM sodium chloride, Thermo Fisher). Add 5mL of binding buffer to equilibrate the column and allow the solution to drain. Apply the diluted sample to the column. Wash the column with 15mL of binding buffer and allow the solution to drain. Elute antibodies with 1mL of glycine-HCl (pH2.0, Nacalai), collecting fractions into each of 100μL neutralization buffer (1M Tris-HCl, pH 8.5, Nacalai)-containing tubes to get eluted B2E5 Ab. Then, the B2E5 was concentrated, and the solvent was replaced with PBS using the centrifugal concentrator (Vivaspin turbo 15).

I investigated the protein elution conditions and examined the elution performance of glycine-HCl buffer with diverse pH values range from 1.0 to 3.0. It was determined that the antibody could only be eluted when the pH was 1.3 and 2.0. To assess whether the eluted antibody was functional, I carried out immunostaining on E6 cells using eluted B2E5 antibody and discovered that the antibodies eluted under both pH conditions were able to specifically recognize E6 cells (Figure 1B).

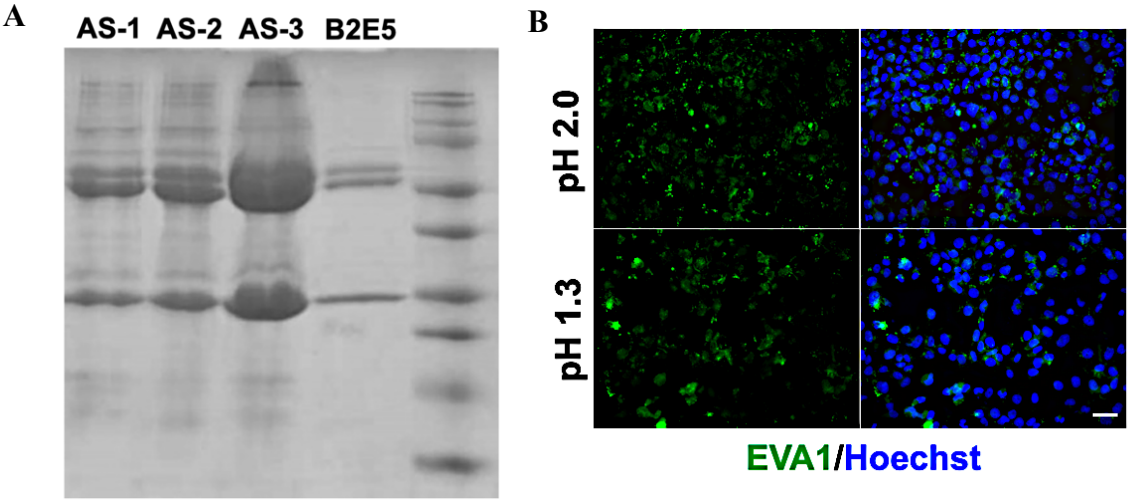

Figure 1: Exploration on conditions for B2E5 purification.

(A) Representative Western blotting results showed the presence of the B2E5 antibody in the ascites (AS) obtained from different individual mice. (B) Representative immunostaining images of E6 cells with the B2E5 antibody eluted under different pH conditions. Scale bar: 50 μm.

Cell killing assay

ADCC assay was performed using Daudi-EVA1, MKN28 human gastric cancer cell line that expresses EVA1 endogenously, and GICs. Daudi-EVA1 and MKN28 ($1x10^6$ cells) were labeled with 10 μg/ml Calcein-AM (Nacarai Tesque) and $1x10^4$ cells/well were then incubated with various concentration of a set of Abs in 96-well plate. Rituximab was used as a positive control. The effector cells ($1x10^5$ cells), mouse FcγRIII-expressing KHYG-1 cells, were added into each well. After centrifugation, calcein in the culture sup released from the labeled target cells was measured using ARVO (Perkin Elmer).

CDC assay was performed using Daudi-EVA1 and MKN28. The target cells were labeled with Calcein-AM as used in the ADCC assay and then incubated with a set of antibodies and the Low-Tox-M rabbit complement (1:64) (CEDARLANE Lab) in 96-well plate. After centrifugation, calcein in the culture sup was measured using ARVO.

We also conducted B2E5-dependent cytotoxicity assays on GICs using a combination of B2E5 and anti-mouse IgG conjugated with saporin (5 nM, Mab-ZAP, Advanced Targeting Systems).

Flow cytometry

hGICs were immunolabeled with either B2E5 or mouse IgG Ab (1 μg/mL; Cosmo Bio, 0107-01), following with Alexa 488-conjugated goat anti-mouse IgG (1:100; Molecular Probe). The cells were subsequently analyzed on a FACS Canto II (BD Biosciences) using a dual-wavelength analysis (488 nm solid-state laser and 638 nm semiconductor laser). Propidium iodide–positive (i.e., dead) cells were excluded from the analysis.

ADC generation

B2E5-ADC and control IgG-ADC were generated using GlyCLICK™ ADC kit MMAE and Antibody MMAE Conjugating kit (GENOVIS and CellMosaic, respectively). To generate B2E5-ADC, the N-glycans on Fc of antibodies were hydrolyzed to the GlcNAc, to which azide was then attached. Finally, MMAE was conjugated to the azide. For IgG-ADC, IgG was labeled with MMAE using a valine-citrulline p-aminobenzylcarbamate liker. Both B2E5-ADC and IgG-ADC were purified using the Fc column. Then, both the B2E5-ADC and IgG-ADC were concentrated to 2 mg/ml and the solvent was replaced with PBS using the centrifugal concentrator (Vivaspin turbo 15).

Brain tumorigenesis

GICs or ELuc-GICs (10^5 cells) were suspended in 5 µL of culture medium and injected into the brains of male nude mice (10- to 12-week-old) under anesthesia with a mixture of medetomidine, midazolam and butorphanol. The stereotactic injection coordinates were 2 mm forward from the lambda, 2 mm lateral from the sagittal suture, and 4 mm depth. Fifteen days after ELuc-GIC transplantation, 5 µL of B2E5-ADC, B2E5, IgG-ADC or IgG, each at a concentration of 2 mg/ml, was directly injected into the tumor-bearing brain twice per week, for a total of four injections. Body weight was measured every 3 days, starting from two weeks after transplantation.

The injection depth between 2 and 5 millimeters was tested. 5 ul of 1% fast green (Wako) into the brains of C57BL/6 mice at different depths (Figure 2). Based on the dye distribution, it was determined that a 4-millimeter injection depth was more appropriate.

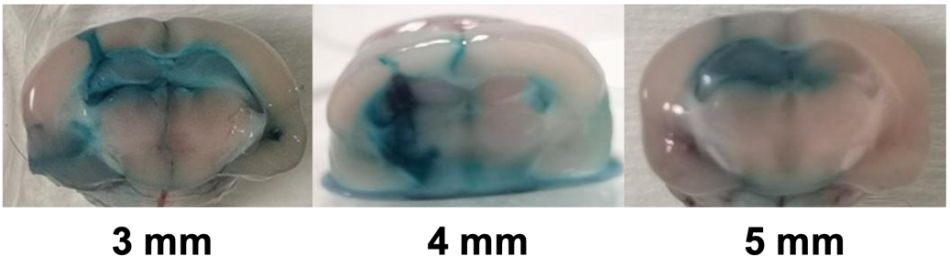

Figure 2: Exploration on conditions of Injection Depth

Pictures of mouse brains after being cut transversely along the injection holes, where 1% fast green was injected into the mouse brains using a syringe at different depths: 3 millimeters (left), 4 millimeters (middle), and 5 millimeters (right).

Cannula administration method has also been attempted (Figure 3). However, due to its short retention time on the mouse brains (most of the cannulas detached approximately two weeks later), I finally abandoned this method.

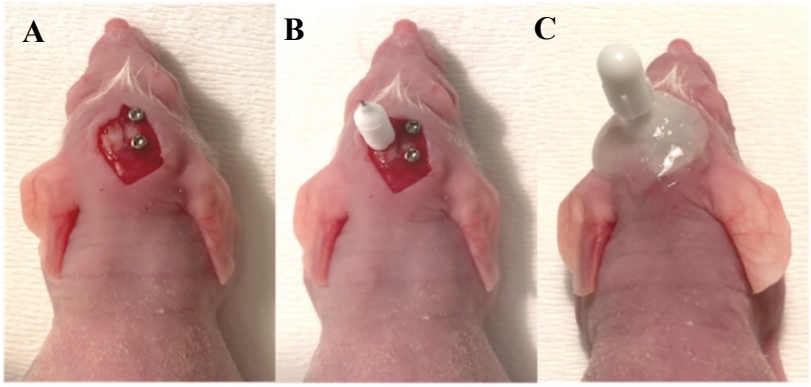

Figure 3: The process of cannula installation.

(A) Dig holes and install fixing screws. (B) embed the Guide. (C) Fixed with teeth cement and wait for recovery.

Bioluminescence Imaging

Firstly, to confirm the successful construction of Eluc-GICs, I examined the presence of Luc signal *in vitro* with different cell numbers (Figure 4). GICs were resuspended in 100 ul culture medium and co-cultured with 10 ul D-luciferin (final concentration 150 ng/ml, Promega) in the dark for ten minutes. The intensity of luciferase activity was measured as total photon flux (photons/sec, p/s) using Living Image 4.3.1 software (PerkinElmer)

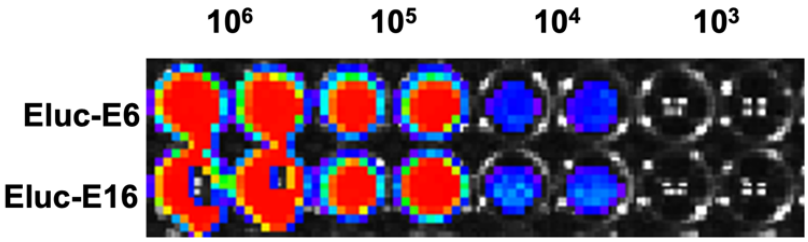

Figure 4: *In Vitro* bioluminescent assay of Eluc-GIC.

Bioluminescent images of Eluc-GICs cells with different cell numbers (Eluc-E6, upper; Eluc-E16, lower)

Subsequently, I explored the observation conditions for the Luc signal *in vivo*. One week after Eluc-E6 transplantation, mice were anesthetized using isoflurane and given intraperitoneal injections of D-luciferin (Promega, 150 mg/kg body weight). The intensity of luciferase activity was measured after D-luciferin injection using Living Image 4.3.1 software (PerkinElmer).

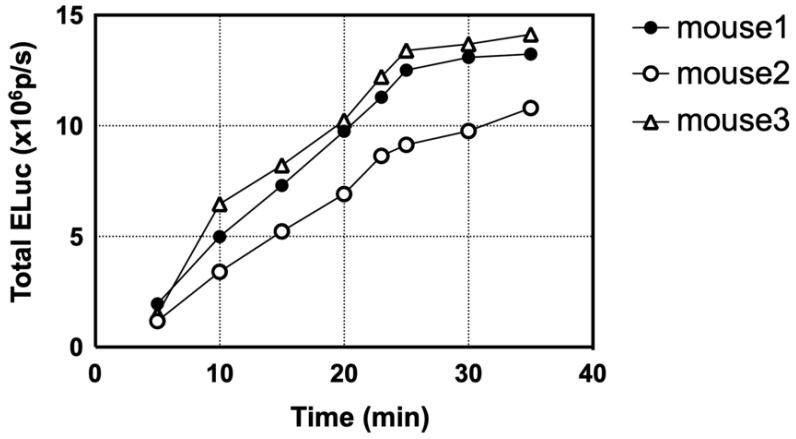

Figure 5: Bioluminescent assay of Eluc-E6 *in vivo*.
A line graph showing the change of luc signal in the brains of Eluc-E6-bearing mice over time following intraperitoneal injection of D-luciferin.

Cell viability
To examine cell proliferation/death, MTT was performed. hGICs (1×10^3 cells/well) were cultured on a 96-well plate for 72 hours. As a background control (0% control), TritonX-100 (final concentration 0.2%, Nacalai) was added to the control wells. MTT (5 mg/ml; Wako Pure Chemical) was added to each well (5 ul), and the cells were incubated for 2.5 hours. The culture medium was replaced with 100 ul of DMSO (Nacalai), the cells were dissolved, and absorbance was measured at 570 nm with a Benchmark microplate reader (Bio-Rad). Cell viability was quantified as follows: Cell viability (%) = (sample- 0%)/ (100% - 0%) *100, where sample is the sample absorbance, 0% is the average 0% control absorbance, and 100% is the average 100% control absorbance.

H&E Staining
The mouse brain sections were incubated in hematoxylin solution for 4 minutes at room temperature and were rinsed with distilled water for 15 minutes to remove excess stain. Subsequently, the slides were incubated with eosin solution for 2 minutes. Then, the slides were dehydrated in 70%, 95% and 100% EtOH (Wako), and clear in Neo-Clear (HX17444743, Sigma), sequentially. Finally, they were covered by Neo-Mount (HX86361616, Sigma). H&E staining data were captured by BZ800 microscope (Keyence).

Immunohistochemical analysis
Immunocytochemistry was performed as described below. Cells were fixed with 4% PFA solution at room temperature for 10 minutes and pretreated with a blocking buffer containing 10% FBS in 0.3% Triton X-100 (Wako) in PBS at room temperature for 30 minutes and then incubated with primary antibodies which were diluted in the blocking buffer at room temperature for 2 hours. After washing the sample 3 times in PBS buffer, the cells were incubated with the secondary antibodies at room temperature for 1 hour.

Immunostaining of paraffin-embedded human brain-tumor sections (6 μm thick) was performed. The paraffin slides were dewaxed in Neo-clear (Sigma Aldrich) at

room temperature for 10min. Then the slides were dehydrated in 100%, 95% ,80% EtOH (Wako) and Ac MilliQ for 1 minute at room temperature.

Antigens were retrieved by HistoVT One (Nacalai). The sections were permeabilized with 0.3% TritonX-100 in PBS for penetration, then treated with a blocking buffer (10% FBS in 0.3% Triton X-100 in PBS) for 1 hour and incubated with primary antibodies for at room temperature for 2 hours. After washing the sample 3 times in PBS buffer, the sections were incubated with the secondary antibodies at RT for 1 hour.

All nuclei were counterstained with Hoechst 33342 (1 μg/ml, Thermo Fisher). Fluorescence images were obtained using an AxioImager A1 microscope (Carl Zeiss) and a C2/Ti-E/PFS confocal microscope system (NIKON).

Human brain tumors

Human brain-tumor sections samples were obtained from Ehime University Hospital with the patients' consent according to the Research Ethics Committee guidelines and were used in compliance with the research guidelines of the Ehime University Graduate School of Medicine and the Institute for Genetic Medicine of Hokkaido University (1208009 and 13-0002(4))

Antibodies

The following Abs were used to detect antigens: mouse monoclonal Abs B2E5 and C3 (1 μg/ml), rabbit polyclonal anti-EVA1 (10 μg/ml), rabbit polyclonal anti-MPZL2 (1:100, Proteintech), biotinylated goat polyclonal anti-human SOX2 (1:200, R&D), chicken anti-GFP (1:500, Abcam), rat monoclonal anti-F4/80 (1:150, Invitrogen), rabbit polyclonal anti-cleaved Caspase 3 (Casp3) (1:1000, Cell Signaling Technology) and mouse monoclonal anti-human mitochondria (1:100, Merck Millipore). The Abs were detected with goat anti-mouse IgG-Alexa 488 (1:1000, Molecular Probes), goat anti-chicken IgG-Alexa 488 (1:1000, Molecular Probes), streptavidin-Cy3 (1:200, Thermo Fisher), goat anti-mouse IgG-Alexa 594 (1:1000, Invitrogen), goat anti-rat IgG-Alexa 594 (1:1000, Invitrogen) and goat anti-rabbit IgG-Alexa 594 (1:1000, Molecular Probes).

Dot-blot Analysis

Total protein was prepared from cells transfected with a set of EVA1 expression vectors using sonication (ULTRAS.HOMOGENIZER VP-5S, TAITEC), in

accordance with the manufacture's protocol. Samples were diluted in PBS with a protease inhibitor cocktail (5 μg/μl, Nacalai Tesque). Ten micrograms of each sample were spotted onto a nitrocellulose membrane (0.45 μm, Bio-Rad) and allowed to dry at RT. The membrane was incubated with a blocking buffer containing 5% skim milk and 0.1% Tween 20 (Wako) in Tris-buffer saline (Nacalai) at RT for 1 hr. The membrane was then incubated with B2E5 (1 μg/ml) suspended in the blocking buffer at 4°C overnight. B2E5 was detected with HRP-conjugated anti-mouse IgG (1:1000, BioLegend) at RT for 1hr. An ECL detection system (Bio-Rad) was used for detection. The membrane was also stained with Ponceau S (Abcam) to confirm that protein was successfully blotted.

RT-PCR/qPCR

Human glioma samples (0.5 cubic centimeter) were crushed using a MagNA Lyser (Roche). Total RNA was prepared with the QuickPrep mRNA Purification Kit (GE Healthcare). Total RNA (200 ng) was reverse transcribed with ReverTra Ace (TOYOBO). Firstly, the RNA was denatured at 65°C for 5min, then the reaction mixture (10 μl) was prepared as follows: 5×RT Master Mix (2 μl), RNA (200 ng), Nuclease-free water. Reverse transcription protocol: 37°C for 15 min, 50°C for 5 min, 98°C for 5 min.

qPCR was carried out in a 20 μl reaction mixture that contained 3 μl of cDNA as template. Gene expression was analyzed using THUNDERBIRD SYBR qPCR Mix (Toyobo Co. Ltd.). All the expression values were normalized against 18S ribosomal RNA expression levels. PCR protocol: initial denaturing at 95°C for 1 min, 40 cycles of 95°C for 15 s, 60°C for 30 s, and melting curve analysis was applied on a StepOnePlus (Applied Biosystems) coupled with StepOne software. Primers used are as follows: *18S*, forward, 5′-ACCCGTTGAACCCCATTCGTGA-3′; reverse, 5′-GCCTCACTAAACCATCCAATCGG-3′; EVA1, forward, 5'-TGAATTCGCCACCATGTATGGCAAGAGCTCTACTC-3'; reverse, 5'-AGTCGACTTAGTCTGTGTCTTCTAAATAAACA-3'

Statistical analysis

Statistical analyses were performed using the *t*-test, Two-way Anova and log-rank (Mantel-Cox) test. The survival data were analyzed for significance using Kaplan-Meier methods with GraphPad Prism version 9 software (P values were calculated with the log-rank test). The result significance was indicated as * $p < 0.05$; ** $p <$

0.01; *** $p < 0.001$; **** $p < 0.0001$; ns, not significant. The error bars represent mean values ± SD.

Results

EVA1 is expressed in gliomas and other malignant tumors

In our preceding study, it was discovered that the high expression of *EVA1* correlates with the prognosis of GBM patients. The cBioPortal Data indicated that the prognosis of GBM patients with elevated *EVA1* mRNA levels was poorer in comparison to others. The median survival of patients with elevated EVA1 was 10.41, while that of the others was 12.98 (Ohtsu et al, 2016). We also identified that *EVA1* is widely expressed in diverse types of gliomas, such as DMG, GG, PA, AO, AA and GBM, except for one AO and two GBM samples (Figure 6A). Immunohistochemical analysis further verified that a small quantity of EVA1-positive cells exists in glioma specimens, DMG (8.3 %), AO (7.6 %), AA (9.9 %), AE (5.4 %), and GBM (9.6 %) (Figure 6B, 6D). Moreover, I found that all EVA1-expressing cells in the GBM specimens were positive for SOX2, a stem cell marker (Figure 6C, 6E). Together, these data imply that targeting EVA1 might be applicable to various forms of glioma.

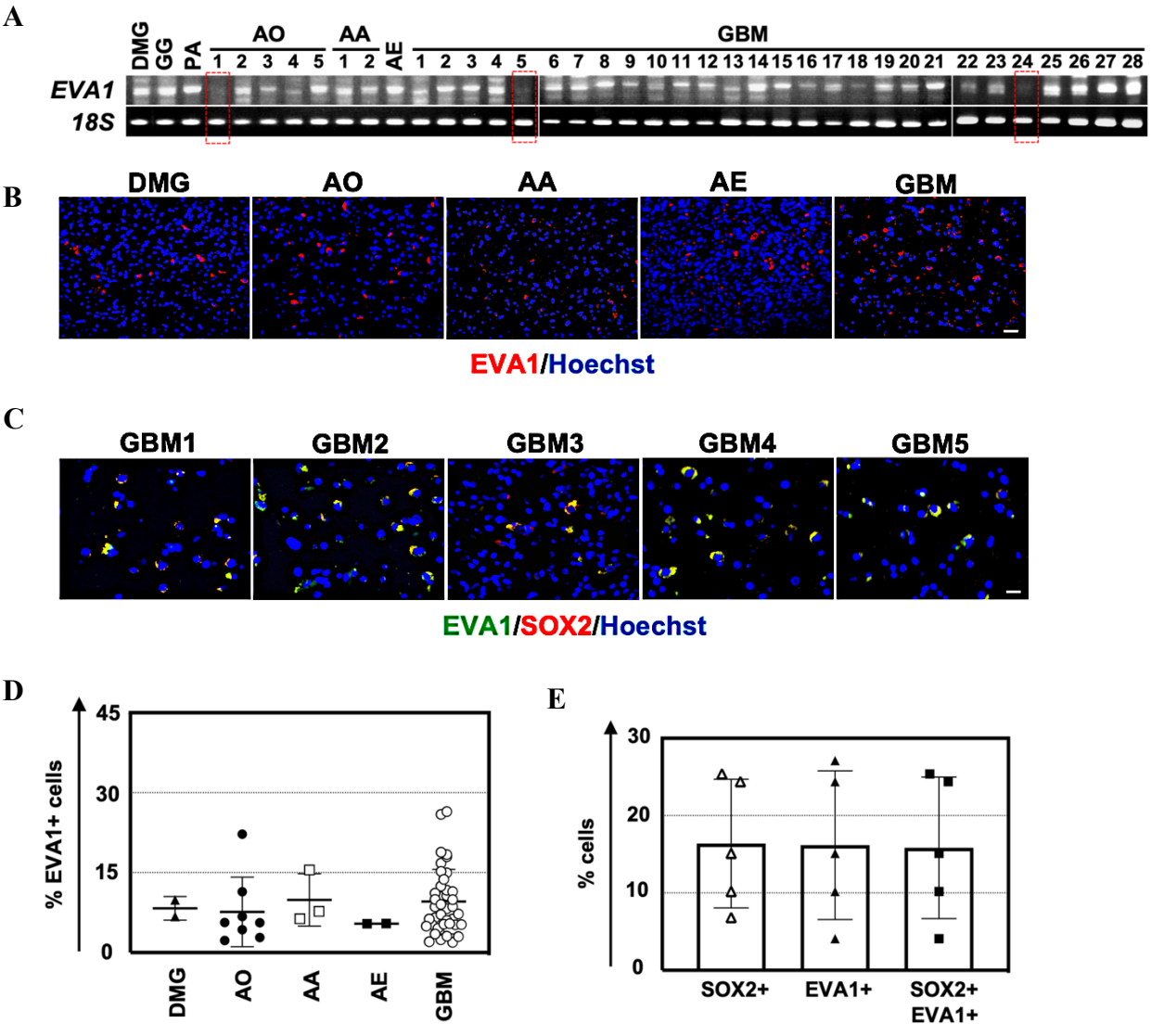

Figure 6: Expression of EVA1 in various types of gliomas.
(A) RT-PCR analysis of *EVA1* in one diffuse midline glioma (DMG), one ganglioglioma (GG), one pilocytic astrocytoma (PA), five anaplastic oligodendroglioma (AO), two anaplastic astrocytoma (AA), one anaplastic ependymoma (AE), and twenty-eight GBM. The 18S gene was used as an internal control. Red dashed squares indicate EVA1-negative glioma specimen. (B) Representative photographs of glioma tissues (DMG, AO, AA, AE and GBM) immunolabeled for EVA1 (red). (C) Representative photographs of GBM sections immunolabeled for EVA1 (green) and SOX2 (red). (D) Quantitative data corresponding to (B). (E) Quantitative data corresponding to (C). All nuclei were counterstained with Hoechst 33342 (blue). Scale bar: 50 μm in B, 100 μm in C.

Prognoscan Data analysis further revealed a significant correlation between increased *EVA1* expression and malignancy in certain cancers, including acute myeloid leukemia, breast cancer, non-small cell lung cancer, and glioma (Figure 7A-D). The Human Protein Atlas (HPA) also illustrated that pancreatic cancer patients with elevated *EVA1* mRNA levels had a worse prognosis than those with lower levels ($p = 0.00011$); more precisely, the median survival for patients with increased *EVA1* expression was 14 months, whereas it was 20 months for those with lower levels (https://www.proteinatlas.org/ENSG00000149573-MPZL2/pathology/pancreatic+cancer). These results suggest that EVA1 could potentially serve as a therapeutic target for various types of malignant tumors.

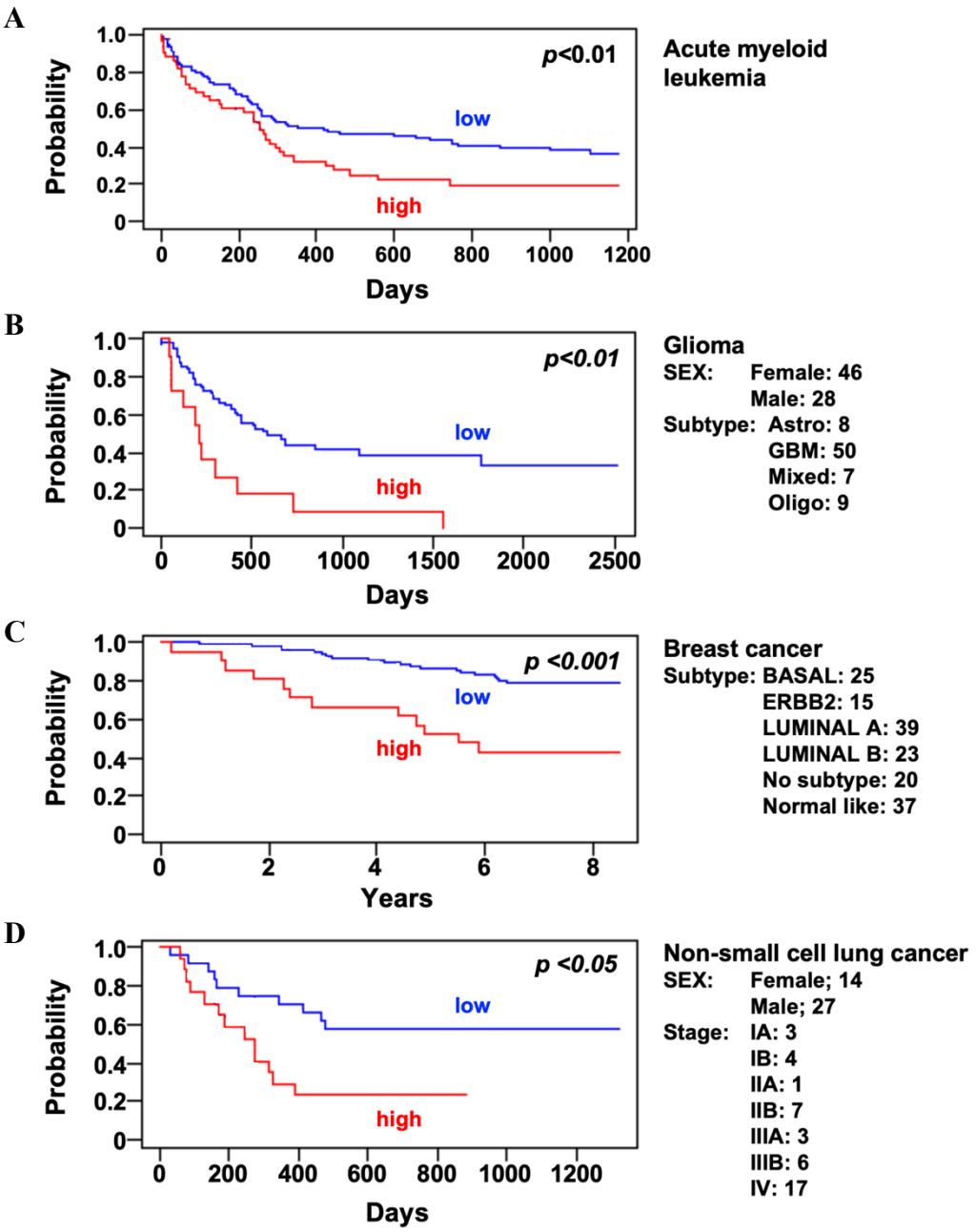

Figure 7: Kaplan-Meier plots of cancer patients based on *EVA1* expression levels
Clinical data from the Prognoscan database indicated that increased *EVA1* expression (red line) correlates with poorer prognosis in acute myeloid leukemia (A), glioma (B), breast cancer (C) and non-small cell lung cancer (D), compared to decreased expression (blue line). Details regarding sex, subtype and stage are provided in panels B-D.

Through the HPA website, we discovered that *EVA1* is moderately expressed in the esophagus and urinary bladder and at low levels in many other tissues (https://www.proteinatlas.org/ENSG00000149573-MPZL2/tissue). I confirmed a

similar trend in Eva1 expression in mouse tissues. Immunohistochemical analysis of mouse tissues revealed a small number of Eva1-positive cells in the liver (0.2%), spleen (1.6%) and lung (2.5%) as well as in brown adipose tissue (5.1%, BAT) that has been shown to express Eva1. However, such expression was not detected in the brain (hippocampus and parenchyma), heart, kidney or skeletal muscle (Figure 8).

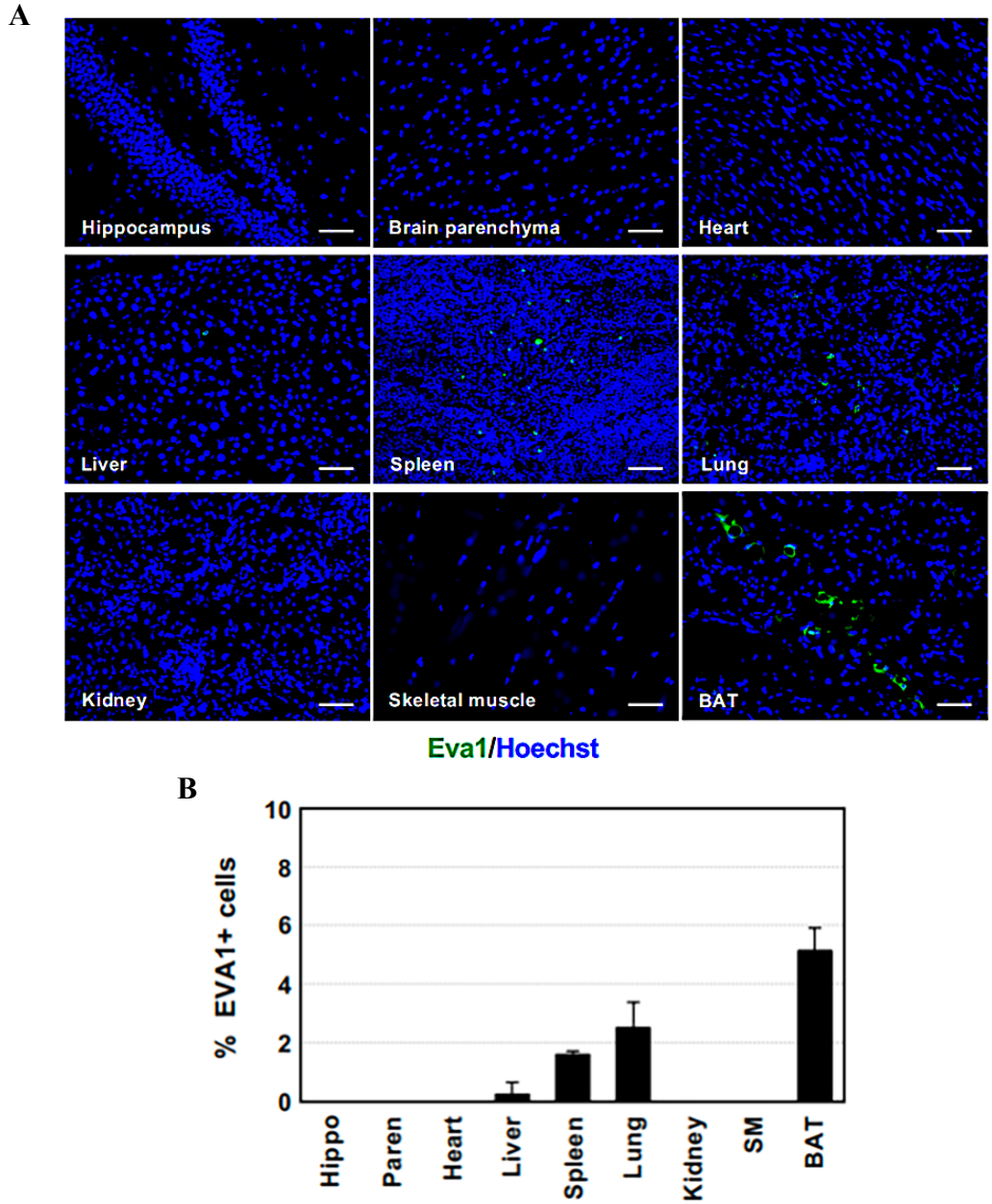

Figure 8: Eva1 expression in adult mouse tissues

(A) Representative mouse tissues, including brain (hippocampus and parenchyma), heart, liver, spleen, lung, kidney, skeletal muscle, and brown adipose tissue (BAT), immunolabeled for Eva1 (green). Adipose tissue served as positive controls for Eva1 immunostaining. All nuclei were counterstained with Hoechst 33342 (blue). Scale bar: 100 µm. (B) Quantitative data corresponding to (A).

B2E5 exhibited high affinity for EVA1

We successfully acquired a set of anti-EVA1 antibodies and evaluated their antibody affinity (Table 1A). The dissociation equilibrium constant (K_D) in antibody affinity is a key parameter that quantifies the strength of binding between an antibody and its antigen. A lower K_D value indicates a higher binding affinity of the antibody for the antigen. Among the candidate antibodies, two anti-EVA1 antibodies, C3-14 (C3) and B2E5-48 (B2E5), demonstrated a high affinity for EVA1 (Table 1B).

A

No.	Antibody	KD (M)	No.	Antibody	KD (M)	No.	Antibody	KD (M)
1	C3-14	$9.06x10^{-9}$	9	B2B11-38	$3.15x10^{-8}$	17	A3F3-11	$7.78x10^{-9}$
2	B1E4-32	$1.52x10^{-8}$	10	B2D11-18	$1.05x10^{-8}$	18	A6A9-36	$5.91x10^{-8}$
3	B2E5-48	$1.17x10^{-8}$	11	A3H5-7	$2.07x10^{-7}$	19	B2B8-41	$4.94x10^{-8}$
4	A1H5-16	$2.18x10^{-8}$	12	B1A8-36	$1.47x10^{-8}$	20	B2B11-16	$2.16x10^{-8}$
5	A5A6-7	$1.34x10^{-5}$	13	A3B10-29	na	21	B2D11-35	$1.17x10^{-8}$
6	A5D11-10	$5.83x10^{-9}$	14	A3B10-36	na	22	B2E9-15	$2.87x10^{-8}$
7	B2C2-41	$2.7x10^{-8}$	15	A3C9-14	$2.51x10^{-7}$	23	B3C2-37	$4.47x10^{-8}$
8	B2F1-22	na	16	A3F3-10	$7.77x10^{-9}$	24	B3C2-42	$3.37x10^{-8}$

B

Ab clone	k_a (1/Ms)	k_d (1/s)	K_D (nM)
C3	9.18×10^5	8.31×10^{-3}	9.06
B2E5	6.89×10^5	8.08×10^{-3}	11.7

Table 1: Antibody Affinity of anti-EVA1 Abs

(A) Binding kinetics of 24 candidate hybridomas for EVA1. na: not available. (B) Association rate constant (Ka), dissociation rate constant (Kd) and dissociation equilibrium constant (K_D) of C3 and B2E5.

Immunoreactivity of B2E5 and C3

Next, we investigated their immunoreactivity towards *EVA1*-overexpressing Daudi cells (Daudi-EVA1) and MKN28 (a low *EVA1*-expressing cell) using flow cytometry. Neither antibody bound to Daudi cells, C3 and B2E5 recognized 84% and 100% of Daudi-EVA1 respectively (Figure 9A). B2E5 also recognized 100% of MKN28, whereas C3 did not bind at all. Remarkably, B2E5 bound more firmly to Daudi-EVA1 than C3, even though C3 had a higher K_D value.

Subsequently, I examined the immunoreactivity of B2E5 to GICs through immunocytochemistry. As illustrated in Figure 9B, B2E5 distinctly immunostained GICs, E6 and E16. To quantify this immunoreactivity, I immunostained GICs with B2E5 and analyzed the cells using flow cytometry. 97% of E6 and all E16 were

immunolabeled with B2E5 (Figure 9C). These data suggested that B2E5 binds to EVA1 on GICs.

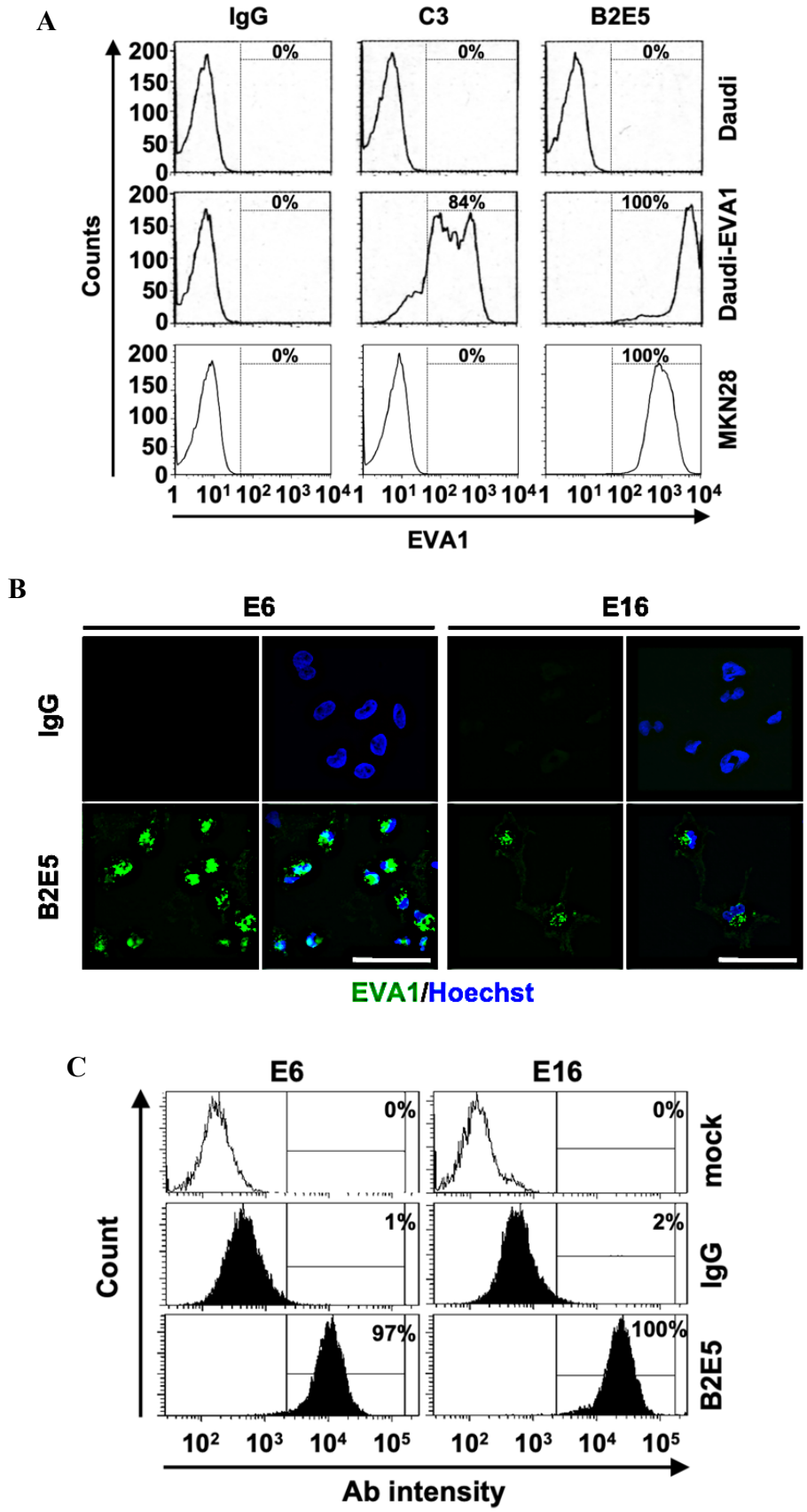

Figure 9: B2E5 recognize Daudi-EVA1 as well as hGICs.

(A) Representative flow cytometry analyses showing the binding of IgG subtype (left panels), C3 (middle panels) and B2E5 (right panels) to control Daudi cells (upper panels), EVA1-expressing Daudi cells (Daudi-EVA1, middle panels) and MKN28 (lower panels). Percentage shows EVA1-positive cells. (B) Representative immunostaining images of GICs, E6 and E16, with control mouse IgG (IgG) and B2E5. (C) Representative data from flow cytometry analysis showing antibody intensity to GICs. IgG was used as a negative control. Percentage shows Ab-labeled cells. Scale bar: 50 μm

B2E5 can target cells with low-level *EVA1* expression

To examine whether high expression of EVA1 is required for B2E5 binding, I used two cancer cell lines, U251 (negative control) and MKN28 (a low EVA1 expressing cell line), as well as E6 (positive control). From the qPCR and flow cytometry results, I confirmed that B2E5 bound MKN28 and E6 in the manner of EVA1 expression level but not U251 (Figure 10). Correctively, these data indicated that B2E5 can target the cells expressing EVA1 at a low level.

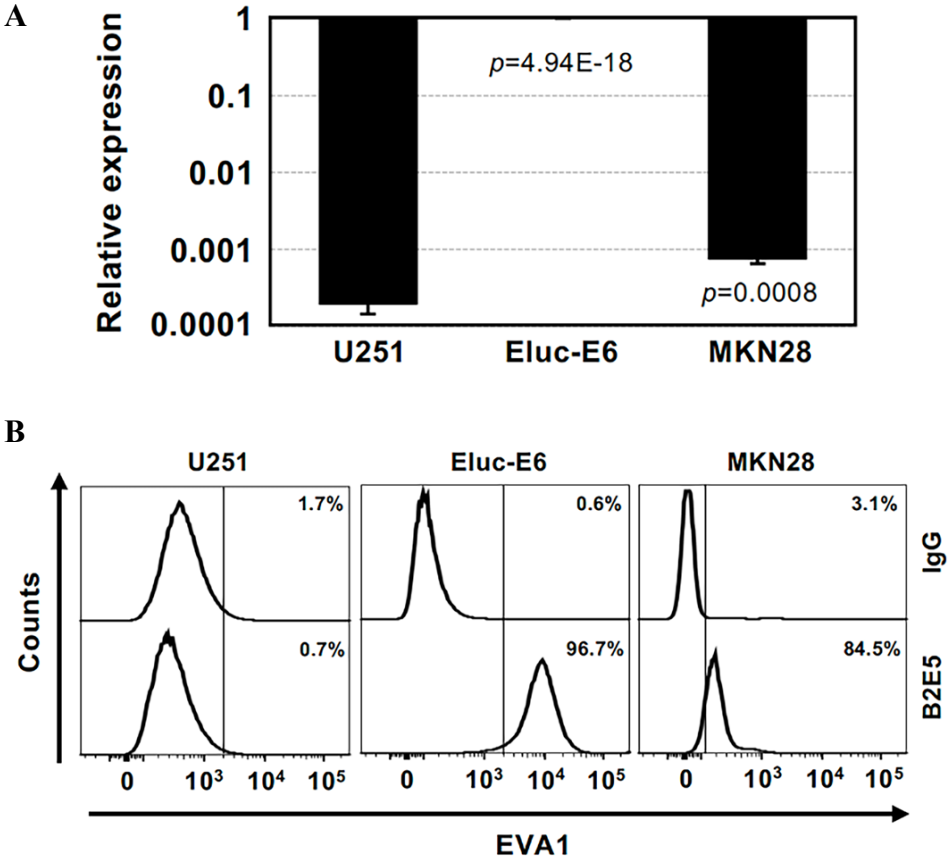

Figure 10: B2E5 can target cells with low EVA1 expression

(A) The expression of *EVA1* in U251, MKN28 and Eluc-E6 was analyzed using quantitative RT-PCR. The mRNA levels are presented as fold changes relative to the mRNA levels in Eluc-E6. (B) Flow cytometry analysis was performed to assess EVA1 expression in U251, MKN28 and Eluc-E6.

B2E5 exhibited strong ADCC and CDC activity *in vitro*

Subtype analysis demonstrated that C3 and B2E5 are IgG1 and IgG2b respectively. In mice, it is well-known that ADCC activity is reliant on the IgG subtype, with the potency ranking as IgG2b>IgG2a>IgG1>>IgG3 (Powell et al, 2008). Meanwhile, CDC activity is at its peak in IgG2b but absent in IgG1. This implies that B2E5 exhibits both ADCC and CDC activities, whereas C3 has a restricted ability with only weak ADCC activity. Indeed, our observations indicated that the ADCC activities of B2E5 towards Daudi-EVA1 and MKN28 were more potent than those of C3 (Figure 11A). The half maximal cytotoxic concentration (CC50) for Daudi-EVA1 was around 5 ng/ml for B2E5 and 9 ng/ml for C3, while the CC50 for MKN28 was approximately 6 ng/ml for B2E5 and 5 µg/ml for C3, respectively. As anticipated, B2E5 also displayed robust CDC activity against Daudi-EVA1, in contrast to C3 which did not (Figure 11B, left panel). The CC50 of B2E5 was about 7 ng/ml. On the other hand, neither B2E5 nor C3 manifested any CDC activity against MKN28 (Figure 11B, right panel). Collectively, these data proposed that B2E5 could be a prospective candidate for an EVA1-targeting therapeutic antibody.

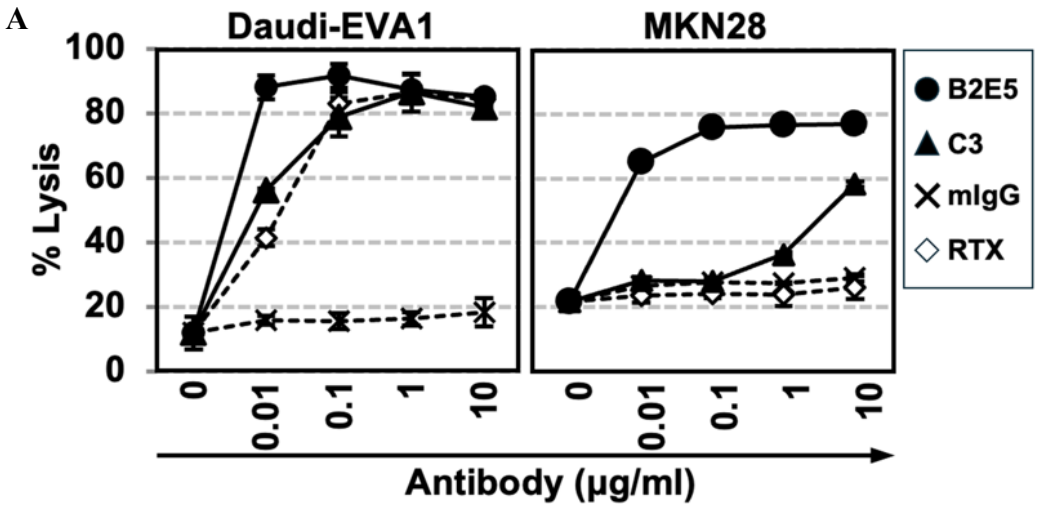

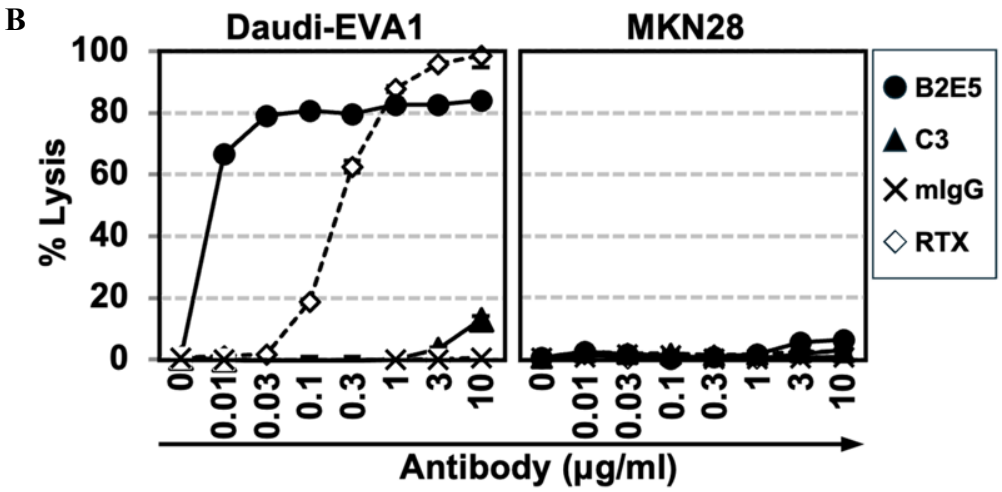

Figure 11: Cytotoxicity of B2E5 to GIC.

(A) Representative data showing ADCC activity of C3 (closed triangle), B2E5 (closed circle), Rituximab (open diamond, dashed line, positive control for cytotoxicity) and control mIgG (cross, dashed line) to Daudi-EVA1 (left) and MKN28 (right). (B) Representative data showing CDC activity of the antibodies as shown in (C). Error bar indicates ±SD.

Proline 72nd is the epitope of B2E5

To investigate the species specificity of B2E5 and C3, we used Biacore assay and found that C3 bound both human and mouse Eva1, whereas B2E5 recognized only human EVA1. To verify the results, I immunolabeled 293T cells expressing either mouse or human EVA1 with C3 and B2E5 and confirmed that B2E5 is a human-specific Ab, while C3 recognized both (Figure 12A).

Although the EVA1 protein is highly conserved between mouse and human, there are 12 amino acid (AA) differences between the two species, suggesting that B2E5 may recognize some of these specific AAs. We focused on those AAs with side chains oriented towards the surface (Figure 12B) and generated four EVA1 mutants: A43V/Q85R/S96V, R33G/V34A/V134L/I135V/E137T, I81M and L68R/P72R, by substituting the candidate AAs with their mouse equivalents. Through immunocytochemical analysis of 293T cells expressing these mutants, I discovered that B2E5 bound to all the mutants except for the L68R/P72R mutant, suggesting that the epitope of B2E5 includes AA68 and AA72 (Figure 12C). To precisely identify the responsible AA, I constructed two single mutants, L68R and P72R, and observed that B2E5 bound to the L68R mutant but not to the P72R mutant. To confirm these results, I carried out a dot-blot analysis and found that B2E5 recognized all the mutants

except for L68R/P72R and P72R (Figure 12D). Together, these data revealed that the 72nd proline residue in EVA1 is the responsible AA for B2E5.

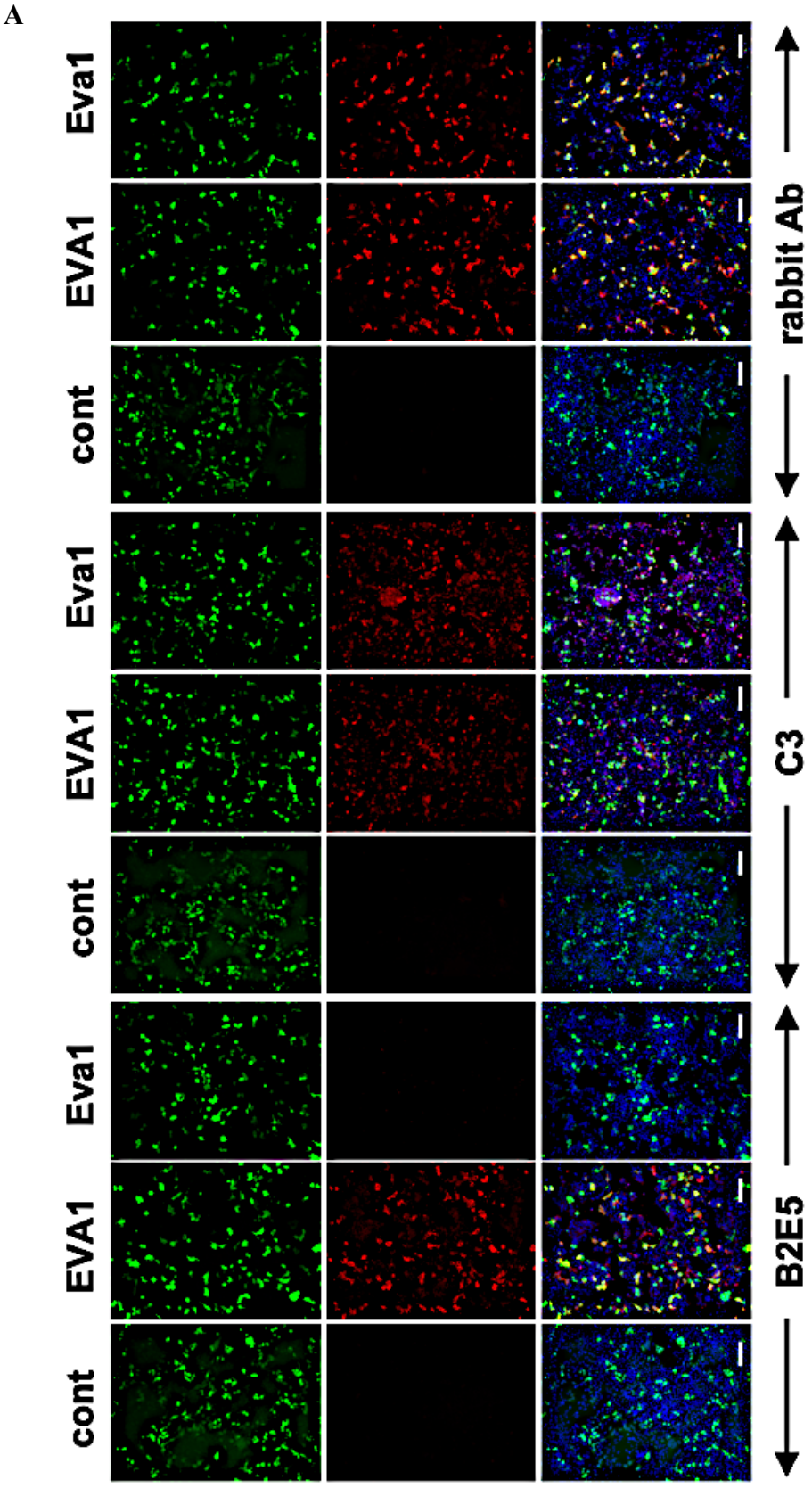

C

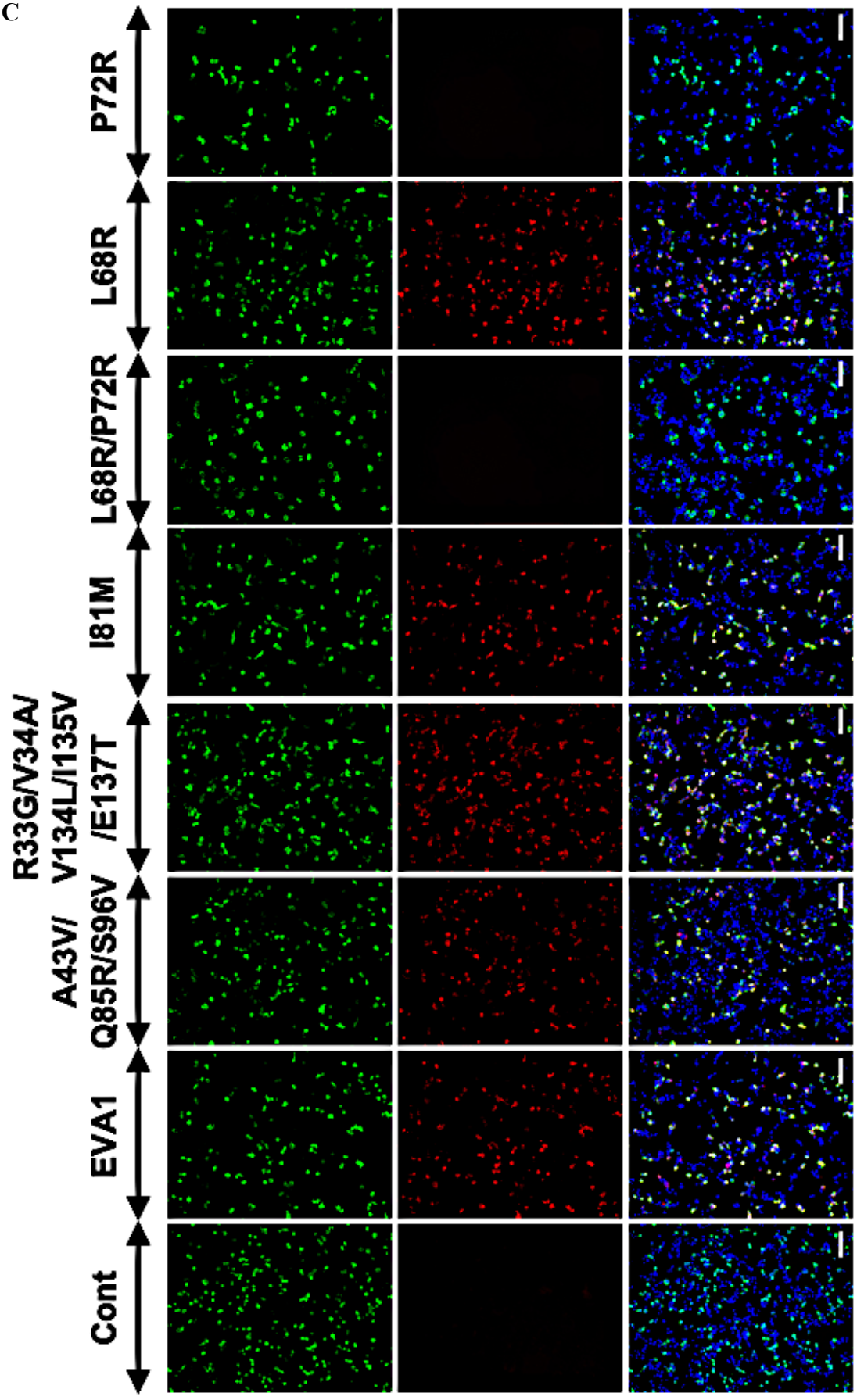
Cont
EVA1
R33G/V34A/
A43V/ V134L/I135V
Q85R/S96V /E137T
I81M
L68R/P72R
L68R
P72R

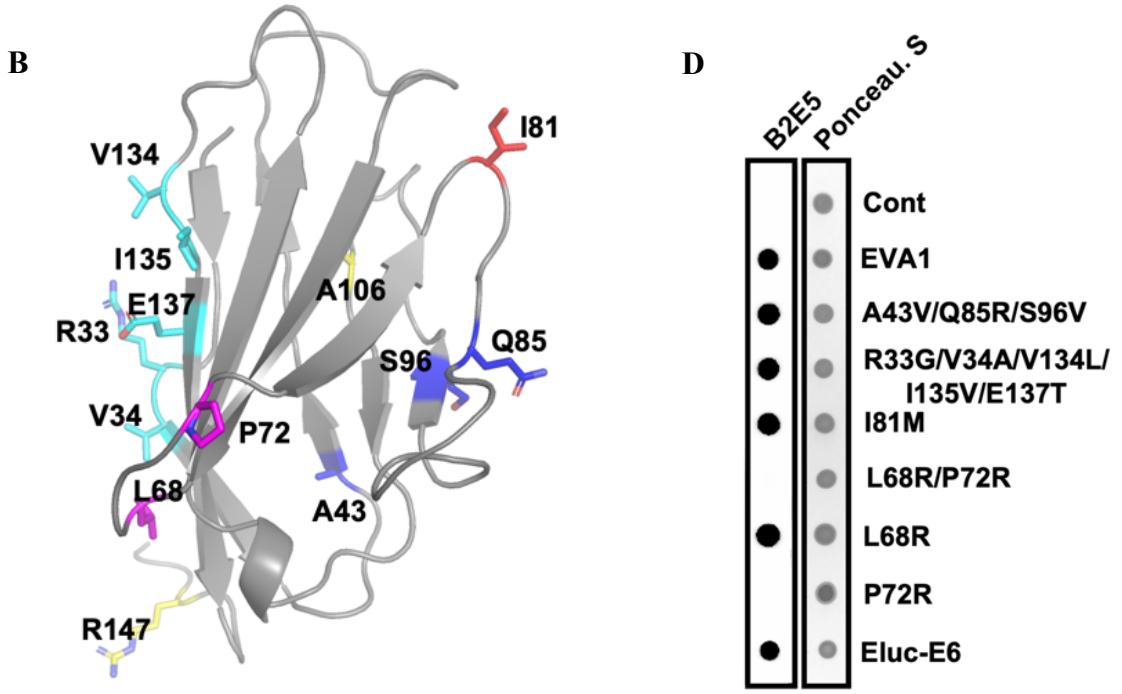

Figure 12: Identification of B2E5 epitope

(A) Immunoreactivity of B2E5, C3, and rabbit polyclonal anti-EVA1 Abs (red) to 293T cells expressing either human EVA1 (EVA1) or mouse Eva1 (Eva1). (B) Immunoreactivity of B2E5 (red) to 293T cells expressing EVA1 and its mutants: A43V/Q85R/S96V, R33G/V34A/V134L/I135V/E137T, I81M, L68R/P72R, L68R or P72R. The pMY-IRES-EGFP vector was used as a negative control (cont), with GFP (green) serving as a transfection marker. (C) Location of mutation sites in the EVA1 structure. AlphaFold2 predicted that R33G, V34A, A43V, L68R, P72R, I81M, Q85R, S96V, V134L, I135V, and E137T are located on the molecular surface. (D) Dot-blot analysis of B2E5 reactivity to EVA1 and its mutants. Ponceau S staining demonstrated the total protein of each sample blotted on the membrane. All nuclei were labeled with Hoechst33342 (blue). Scale bar: 50 μm.

B2E5 alone exhibited no anti-tumor effects *in vivo*.

Given that B2E5 exhibits strong ADCC and CDC cytotoxic effects *in vitro* (Figure 4A, 4B), we aimed to investigate whether B2E5 alone could kill GICs both in culture and in the brain by inducing ADCC or CDC. I first examined whether EVA1 Ab alone affects GIC in culture. I cultured GICs with various concentration of Ab, B2E5, C3, or control mouse IgG (mIgG), and examined their survival/proliferation by MTT assay. I observed that either Ab did not show any cytotoxicity to GICs (Figure 13).

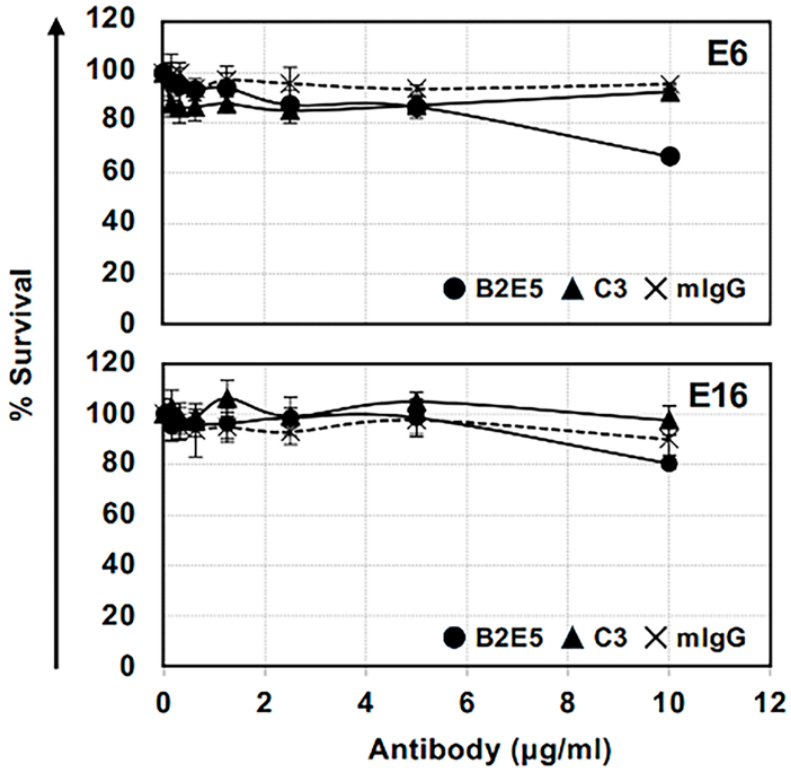

Figure 13: B2E5 and C3 did not induce cell-cycle arrest or cell death in GICs
GICs, E6 (upper graph) and E16 (lower graph), were cultured with various concentrations of control mouse IgG (cross), B2E5 (closed circle) or C3 (closed triangle) for 3 days. Their survival and proliferation were assessed using the MTT assay. Error bar indicates ±SD.

Subsequently, I made use of KSN/Slc nude mice. This strain preserves a certain level of innate immune function. To examine the acute toxicity of B2E5 in mice, I administered single shot of either B2E5 or IgG intravenously but did not observe any obvious influence. Then, I injected the Abs into E6 tumor-bearing mice intravenously (100 μg Ab/25g body weight) six times, made brain sections and examined tumor size by HE staining (Figure 14A). There was no significant reduction in tumor size in brains of B2E5 injected mice compared with those of control Ab injected ones (Figure 14B-C). There was also no significant difference in the survival time between the two groups (Figure 14D). Considering that the number of NK cells, which are the main effector cells for ADCC and CDC in KSN/Slc mice, is relatively small, I switched to BALB/c nude mice, with stronger NK cell activity. I intravenously administered B2E5 and IgG to two E6-bearing BALB/c mice respectively. The percentage of E6 tumor in brain injected with B2E5 was 20.6%, 24.9% respectively. The percentage of

E6 tumor in brain injected with IgG was 15.3%, 21.3% respectively (Figure 14E). Based on the above data, the intravenous injection of B2E5 antibody alone cannot exhibit anti-tumor effects *in vivo*.

A

B

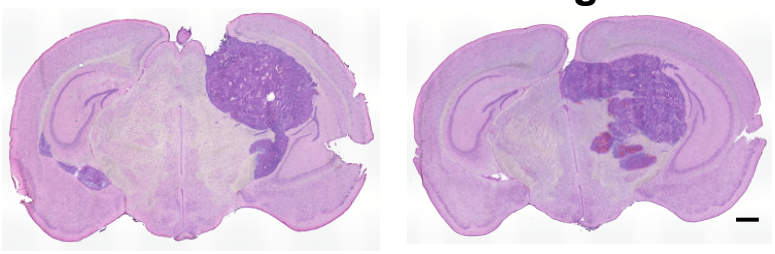

C

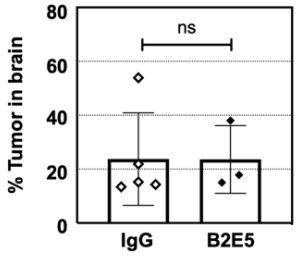

D

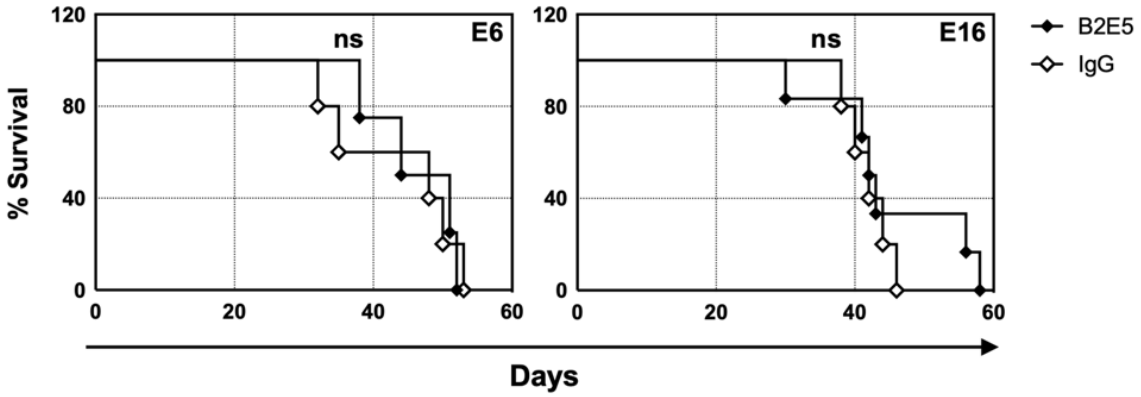

E

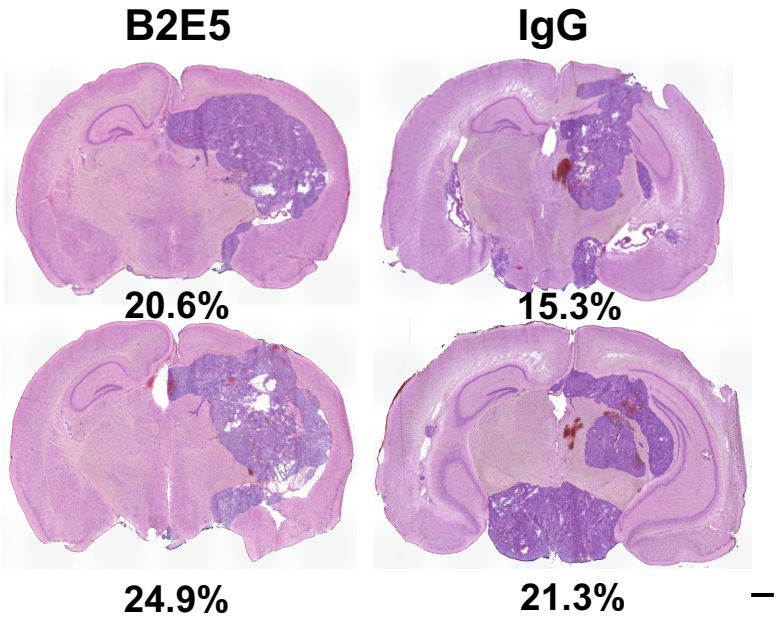

Figure 14: B2E5 itself has no anti-tumor effect *in vivo*.

(A) Experimental procedures examining the anti-tumor effect of IgG, B2E5. (B) Representative H&E staining photographs of coronal sections of E6-bearing KSN/Slc nude mice, which were injected with IgG or B2E5 Intravenously. (C) Quantitative data corresponding to (B). (D) Survival curve for GIC tumor-bearing mice that were injected with IgG (open diamonds) or B2E5 (closed diamonds), N=4~6. Statistical significance was determined by log-rank test. ns, not significant. (E) Representative H&E staining photographs of coronal sections of E6-bearing BALB/c nude mice (n=2), which were injected with IgG or B2E5 Intravenously. Scale bar: 1mm. Statistical significance was determined by log-rank test. Error bar indicates ±SD. ** $p<0.01$, *** $p<0.001$, **** $p<0.0001$. ns, not significant.

B2E5 internalizes into GICs

During the immunocytochemical analysis, I observed that the B2E5 signal on the membrane diminished and spread diffusely throughout the cells over time, which implied its internalization. To confirm this, I cultured E6 with B2E5 for 1, 3, 5, 7 and 9 hours. Subsequently, the cells were fixed and immunostained for B2E5. As illustrated in Figure 15A, it was noticed that B2E5 was internalized from the membrane into the cells as time elapsed, manifesting as spots in the cytoplasm. Confocal microscope analysis further demonstrated that B2E5 was in the cytoplasm of E6 after 7 hours of incubation (Figure 15B).

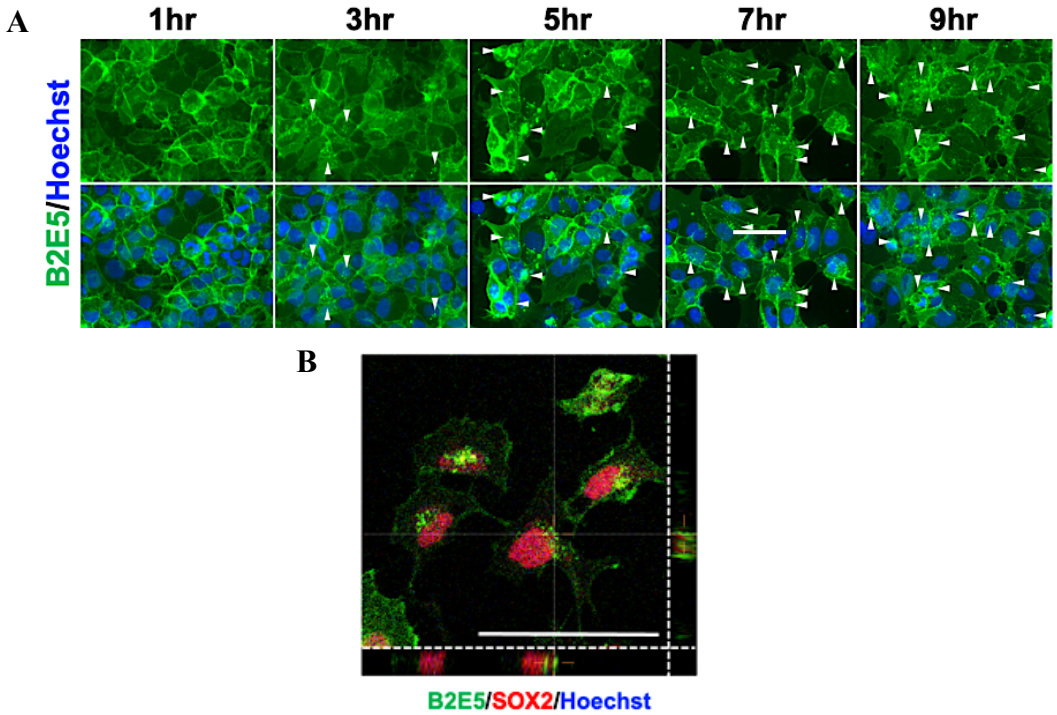

Figure 15: B2E5 internalize into GICs.
(A) Time-course analysis of B2E5 (green) internalization into E6 cells. Arrowheads point B2E5 in the cytoplasm. (B) Representative three-dimensional images, x-y, x-z (bottom) and y-z (right), denoted by white dot line, showing the localization of B2E5 (green) and SOX2 (red, a nuclear protein) in E6 cells. Scale bar: 50 μm.

Given that B2E5 was internalized into E6, I investigated the potential of a B2E5-based ADC by using a combination of B2E5 and the Saporin-conjugated secondary antibody Mab-ZAP (5 nM). This combination effectively eradicated GICs in a B2E5 concentration-dependent manner. In contrast, Mab-ZAP alone, even at a concentration of 20 nM, did not display cytotoxicity towards GICs (Figure 16). These data suggest that B2E5 can be employed to eliminate GICs through ADC *in vivo*.

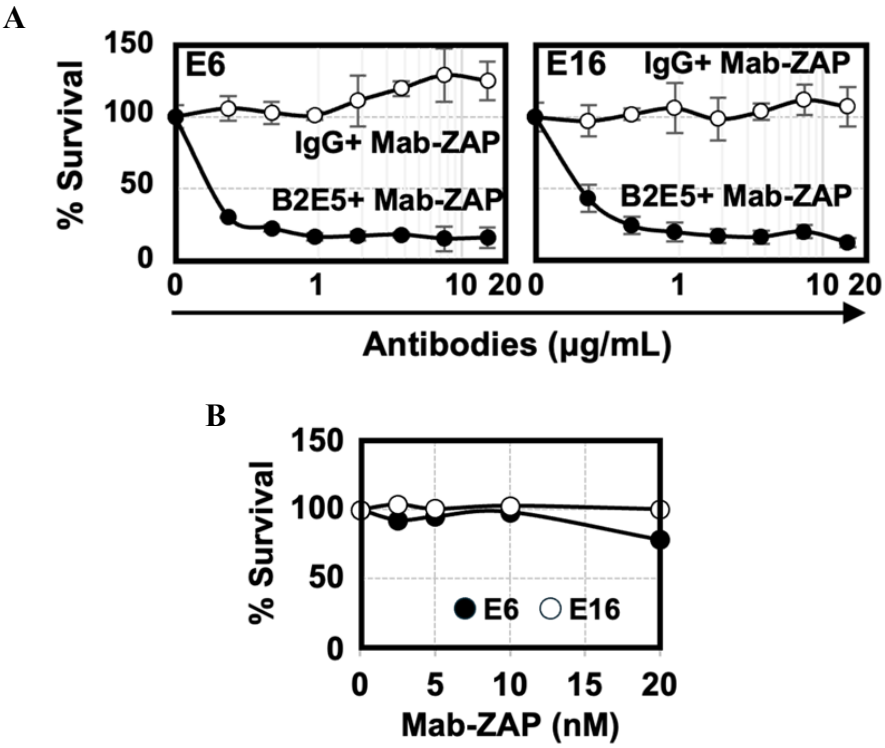

Figure 16: B2E5-conjugated Mab-ZAP kill GICs *in vitro*.
(A) Cytotoxicity of both B2E5+ Mab-ZAP (closed circle) and control IgG+ Mab-ZAP (open circle) to GICs, E6 (upper graph) and E16 (lower graph). (B) Cytotoxicity of Mab-ZAP alone to GICs, E6 (closed circle) and E16 (open circle). All nuclei were labeled with Hoechst33342 (blue). Error bar indicates ±SD. Scale bar: 50 μm.

Cytotoxicity of B2E5-ADC to ELuc-GICs

Considering that B2E5 was internalized into E6 and to evaluate the potential of B2E5 as a therapeutic antibody for GBM, I generated IgG-ADC and B2E5-ADC by conjugating mouse IgG and B2E5 with a potent mitotic inhibitor MMAE respectively. I initially examined the cytotoxicity of these ADCs against ELuc-GICs *in vitro*. Three days after culturing ELuc-GICs with various concentrations of antibodies, IgG, B2E5, IgG-ADC and B2E5-ADC, I carried out the MTT assay and observed a strong cytotoxic effect of B2E5-ADC against ELuc-GICs, while the other treatments did not exhibit similar effects (Figure 17A). To confirm this cytotoxicity, I cultured ELuc-GICs with antibodies, IgG, B2E5, IgG-ADC or B2E5-ADC (at a final concentration of 5 ng/ml) for up to 3 days and immunolabeled the cells for cleaved Caspase 3 (Casp3), a marker for cell death. As depicted in Figure 17B-C, the number of Casp3-positive cells increased over time in both cell types cultured with B2E5-ADC. In contrast, ELuc-GICs cultured with the other treatments showed no Casp3 positivity, except that a small number of Eluc-GICs, Eluc-E6 and Eluc-E16, cultured with IgG-ADC were Casp3+ on Day 3 in all experiments (Figure 17B-C).

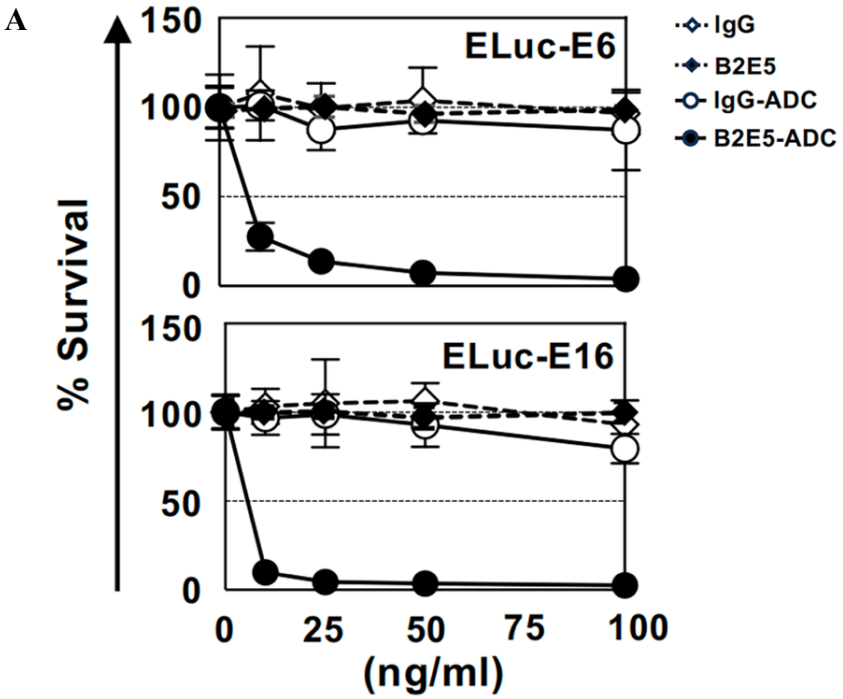

B

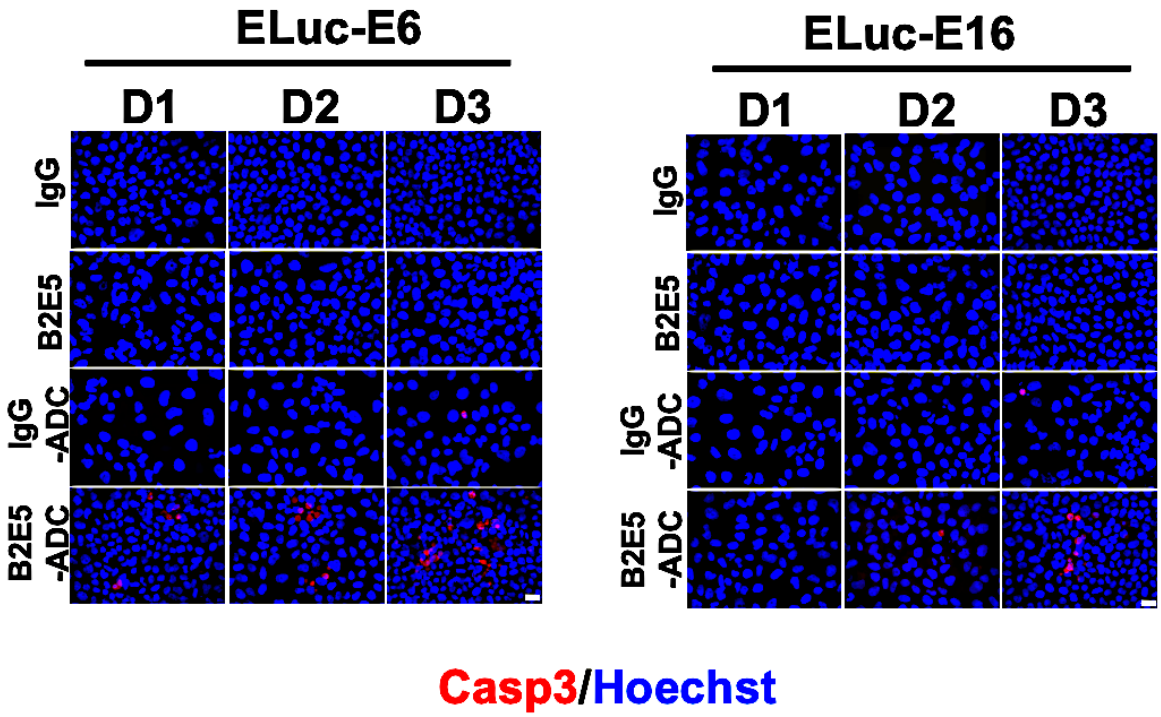
ELuc-E6
ELuc-E16
D1
D2
D3
IgG
B2E5
IgG -ADC
B2E5 -ADC
Casp3/Hoechst

C

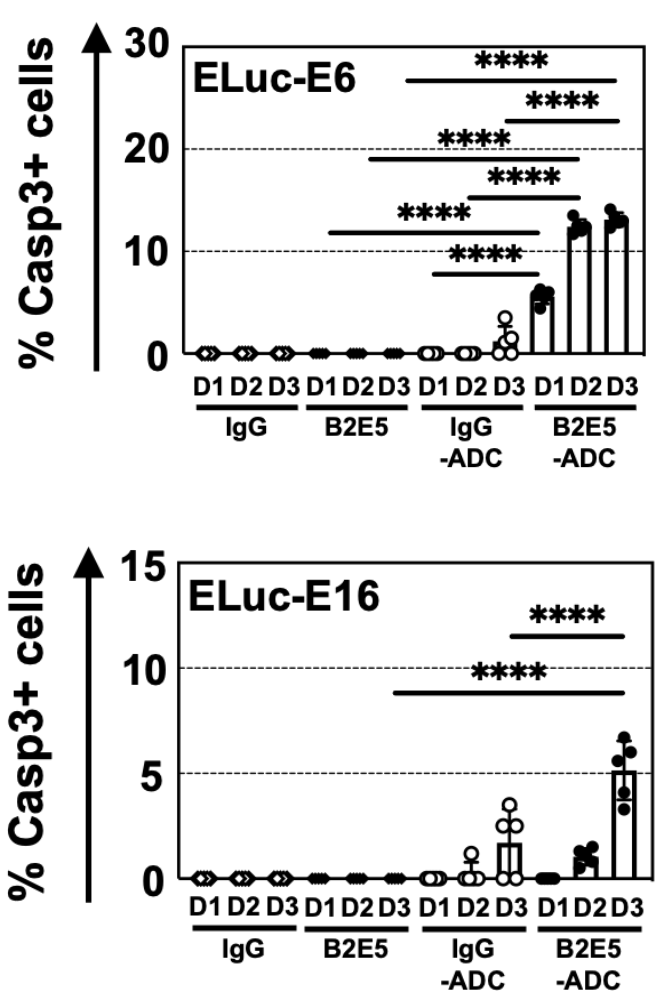
% Casp3+ cells
ELuc-E6
30
20
10
0
****
D1 D2 D3 D1 D2 D3 D1 D2 D3 D1 D2 D3
IgG
B2E5
IgG -ADC
B2E5 -ADC
ELuc-E16
15
10
5
0

Figure 17: Cytotoxicity of B2E5-ADC *in vitro.*

(A) Cytotoxicity of B2E5-ADC to GICs, ELuc-E6 (left graph) and ELuc-E16 (right graph), *in vitro*. IgG, IgG-ADC and B2E5-ADC are shown as open diamond with dashed line, open circles with solid line and closed circles with solid line, respectively. (B) Representative immunostaining images of hGICs with Casp3 which were cultured with IgG, B2E5, IgG-ADC or B2E5-ADC for three days. D1, D2, D3 stand for Day1, Day2, Day3, respectively. (C) Percent of Casp3-positive ELuc-GICs, ELuc-E6 (left graph) and ELuc-E16 (right graph), which were cultured with IgG (open diamonds), B2E5 (closed diamonds), IgG-ADC (open circles) or B2E5-ADC (closed circles) for three days. Statistical significance was determined by Two-way ANOVA. Error bar indicates ±SD. ** $p<0.01$, ***$p<0.001$, ****$p<0.0001$.

Intracranial injection of B2E5-ADC prevented ELuc-GIC tumorigenesis in the brain

Next, I investigated whether B2E5-ADC could prevent tumorigenesis in the brain. Firstly, I compared the anti-tumor effects via three distinct drug administration methods: intravenous injection, intrathecal injection and intracranial injection. It was discovered that only the intracranial B2E5-ADC exhibited significant anti-tumor effects, and both the twice-dose and four-dose regimens showed remarkable anti-tumor activities (Figure 18A). After confirming that injection of either IgG-ADC or B2E5-ADC did not cause any visible toxicity in the mice (Figure 18B), I transplanted ELuc-GICs into the brains of nude mice. Subsequently, I intracranially injected Abs, IgG, B2E5, IgG-ADC or B2E5-ADC four times to optimize the anti-tumorigenic activity. To monitor the ELuc-GIC tumorigenesis, I measured the Eluc activity 13 and 29 days after GIC transplantation. I noted significantly lower Luc activity in GIC tumor-bearing mice injected with B2E5-ADC in comparison to those injected with the other treatments (Figure 18C-D). Moreover, all mice injected with B2E5-ADC survived for over 55 days after ELuc-GIC transplantation, whereas all mice injected with other Abs died around 40 days (Figure 18E). These results attest to the potent anti-tumorigenic activity of B2E5-ADC against GIC brain tumors.

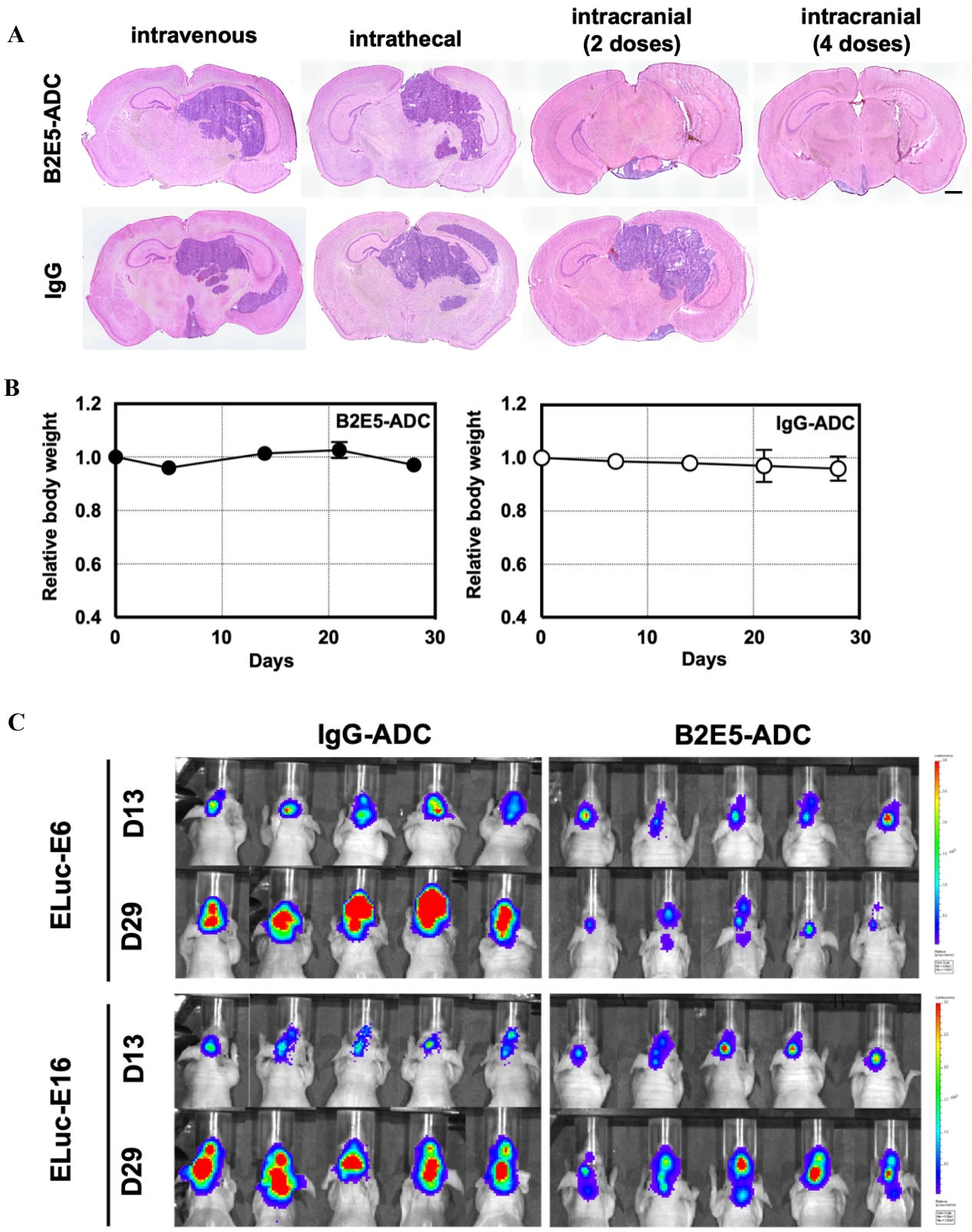
A
intravenous
intrathecal
intracranial (2 doses)
intracranial (4 doses)
B2E5-ADC
IgG
B
Relative body weight
1.2
1.0
0.8
0.6
0.4
0
10
20
30
Days
B2E5-ADC
IgG-ADC
C
IgG-ADC
B2E5-ADC
ELuc-E6
ELuc-E16
D13
D29

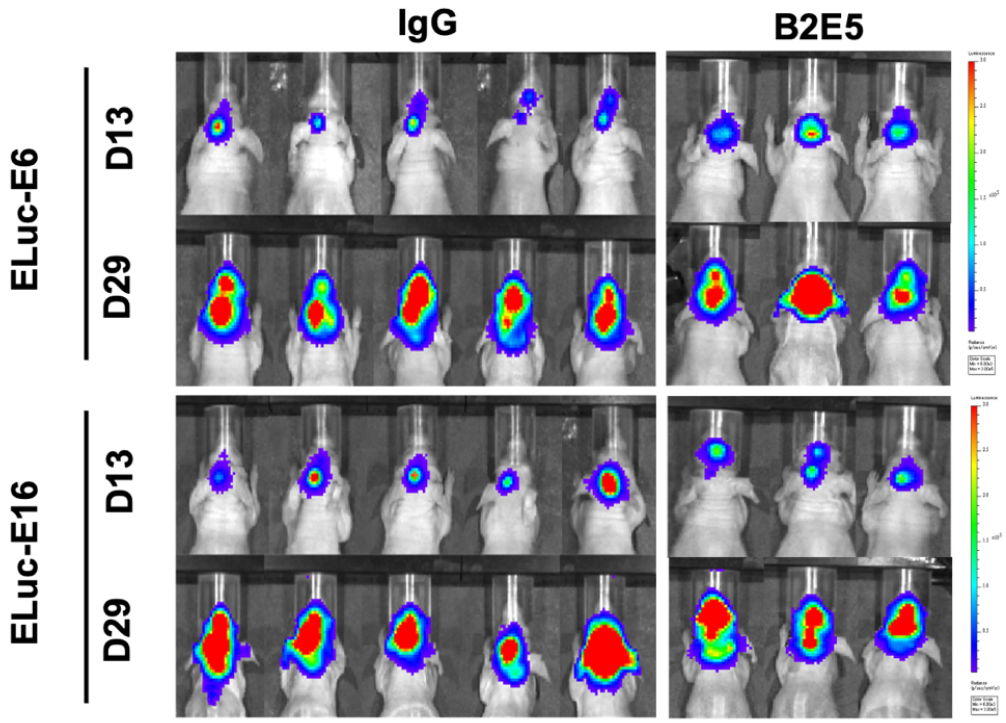
IgG
B2E5
ELuc-E6
D13
D29
ELuc-E16
D13
D29

D

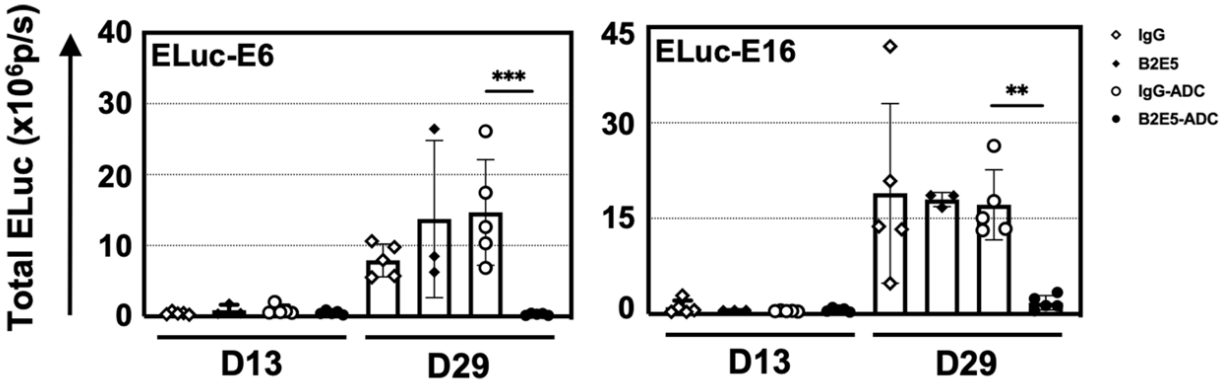
Total ELuc (x10⁶p/s)
ELuc-E6
***
ELuc-E16
**
IgG
B2E5
IgG-ADC
B2E5-ADC
D13
D29
D13
D29

E

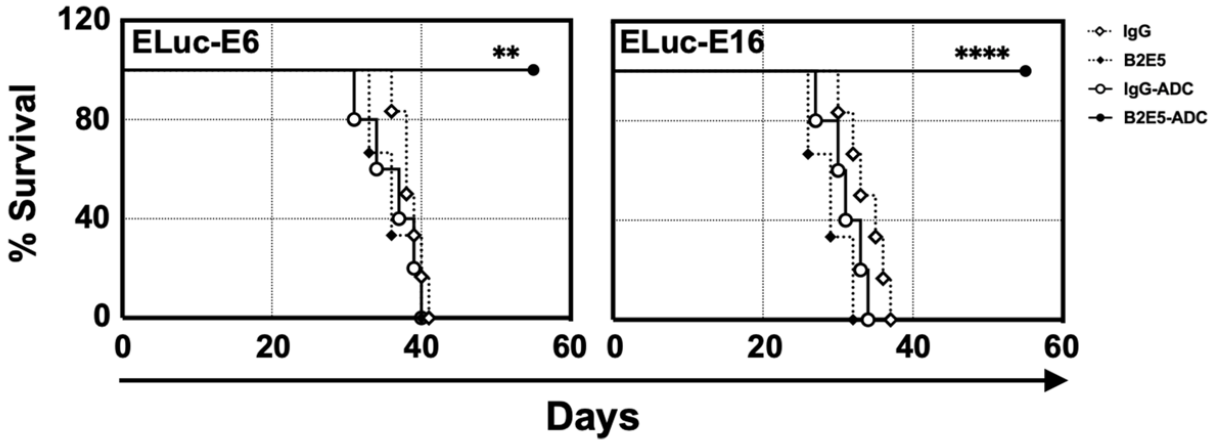
% Survival
ELuc-E6
**
ELuc-E16
****
IgG
B2E5
IgG-ADC
B2E5-ADC
Days

Figure 18: Anti-tumorigenic activity of B2E5-ADC in GIC brain tumor
(A) H&E staining of coronal sections of E6-bearing brains, which were injected with IgG or B2E5-ADC, intravenously, intrathecally and intracranially. Scale bar: 1mm. (B) To investigate the acute toxicity of B2E5-ADC and IgG-ADC, KSN/Slc nude mice (n=3) were injected intracranially with 5 μl (2 mg/ml) of either B2E5-ADC or IgG-ADC. Their health and body weight were monitored at 0, 5, 14, 21, and 28 days after injection. (C) Bioluminescent images of ELuc-GIC brain tumors, ELuc-E6 (upper graphs) and ELuc-E16 (lower graphs), which were injected with IgG, B2E5, IgG-ADC or B2E5-ADC. (D) Quantitative data of total ELuc in C. IgG (open diamonds), B2E5 (closed diamonds), IgG-ADC (open circles) or B2E5-ADC (closed circles). Statistical significance was determined by Two-way ANOVA. (E) Survival curve for GIC tumor-bearing mice that were injected with IgG (open diamonds), B2E5 (closed diamonds), IgG-ADC (open circles) or B2E5-ADC (closed circles). Overall survival was followed up to 55 days (n = 6). Statistical significance was determined by log-rank test and Two-way ANOVA. Error bar indicates ±SD. ** $p<0.01$, *** $p<0.001$, **** $p<0.0001$.

B2E5-ADC treated GIC brain tumor lost GBM pathological features *in vivo*
To further analyze anti-tumorigenic activity of B2E5-ADC, I examined brain sections from the transplanted ELuc-GIC brains that were injected with IgG, B2E5, IgG-ADC or B2E5-ADC, staining them with HE (Figure 19A and 19C). The percentage of ELuc-GIC tumor in the brains injected with B2E5-ADC was significantly smaller than others (Figure 19A, 19B). I observed tumor shrinkage in the brains of tumor-bearing mice injected with B2E5-ADC (Figure 19C IV and VIII), in comparison to those injected with either IgG, B2E5 or IgG-ADC (Figure 19C I - III and V - VII).

Pathological analysis revealed extensive hemorrhage in the brains injected with either IgG, B2E5 or IgG-ADC, while a similar lesion was limited in the brains injected with B2E5-ADC (Figure 19C I'-IV' and V'-VIII'). Additionally, I observed increased hemosiderin deposition, which is a consequence of previous hemorrhages or the infiltration of inflammatory cells such as lymphocytes and macrophages in the brains injected with B2E5-ADC (Figure 19C IV'' and VIII'').

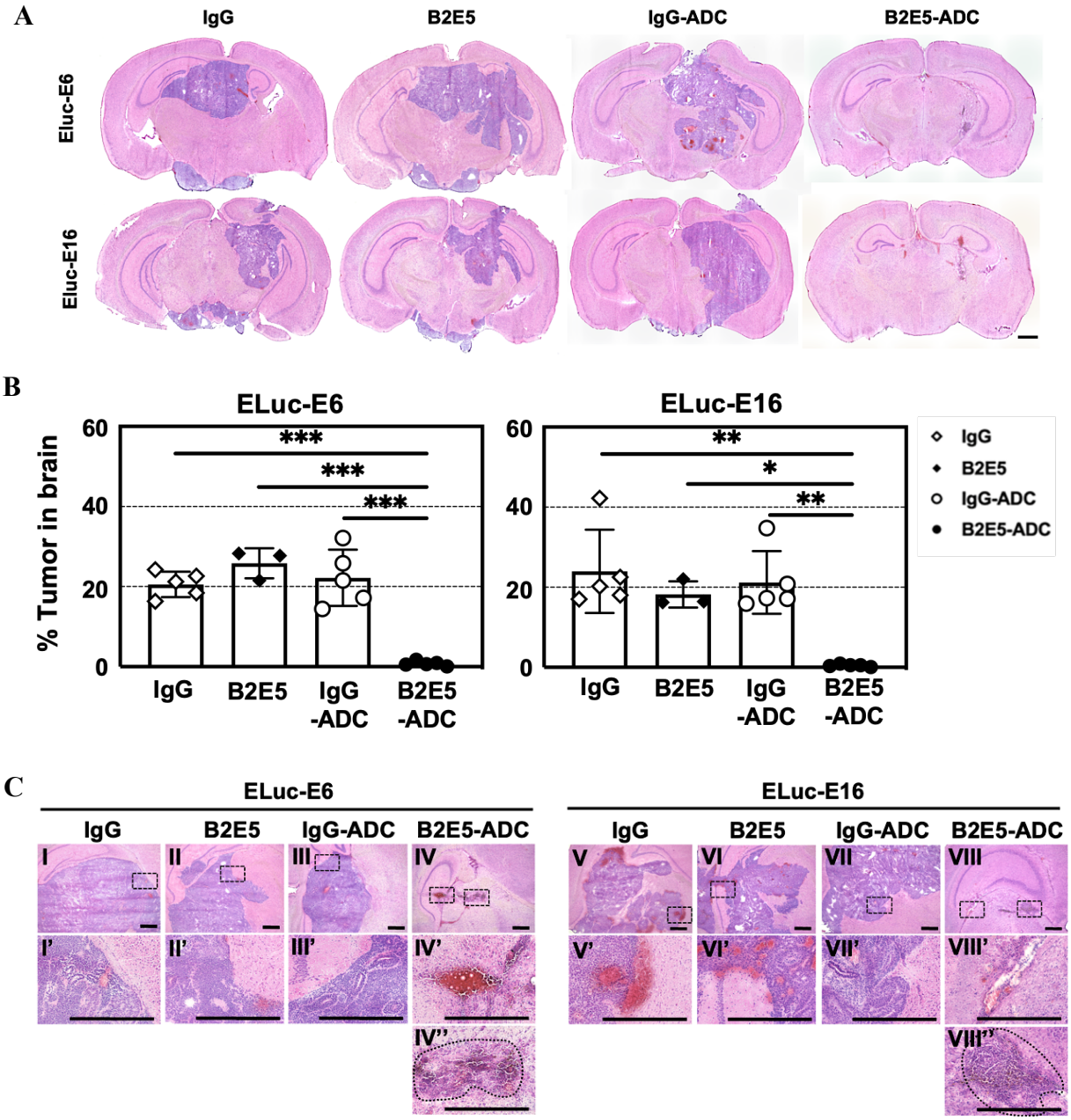

Figure 19: B2E5-ADC treated GIC brain tumor loses GBM pathological features

(A, C) H&E staining of coronal sections of ELuc-GIC tumor-bearing brains, ELuc-E6 (upper graph) and ELuc-E16 (lower graph), which were injected with IgG, B2E5, IgG-ADC or B2E5-ADC. (B) Quantitative data of percent tumor in brain in A. Scale bar: 1 mm in A, 0.5 mm in C. Statistical significance was determined Two-way ANOVA. Error bar indicates ±SD. ** $p<0.01$, ***$p<0.001$, ****$p<0.0001$.

Abundant apoptotic signals and macrophage aggregation post B2E5-ADC treatment

To confirm whether B2E5-ADC killed GICs in the tumor, I immunolabeled brain

sections for the cell death marker Casp3. I observed extensive Casp3+ signal in the brains injected with B2E5-ADC, while there was no signal in the brains injected with IgG, B2E5 or IgG-ADC (Figure 20A). The percentage of Casp3+ cells in ELuc-E6 and ELuc-E16 brain tumors injected with B2E5-ADC was 14.26 ± 3.61% and 10.46 ± 1.91% respectively, while that with IgG-ADC was 0% and 0.44 ± 0.44% respectively (Figure 20B).

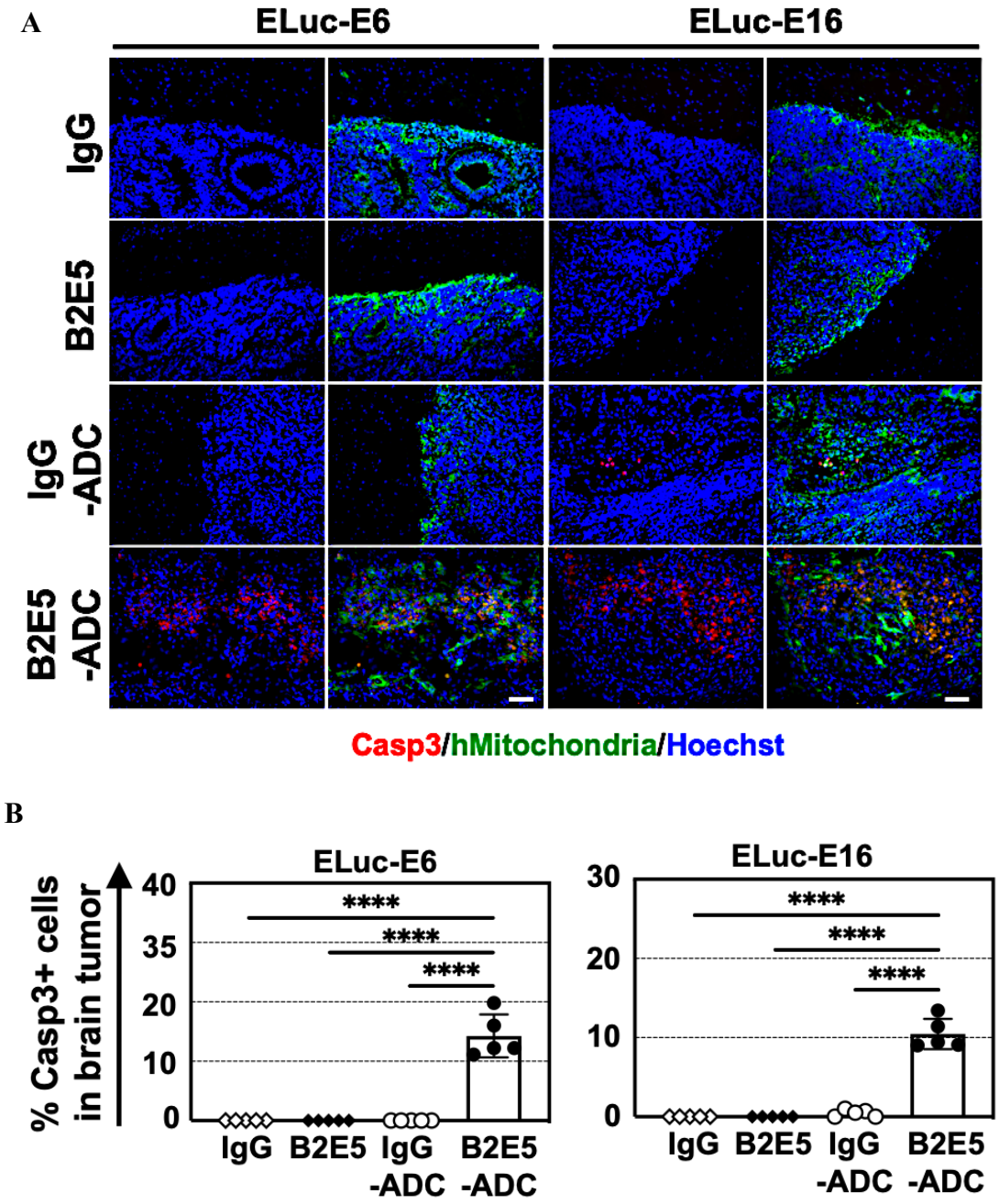

Figure 20: Abundant apoptotic signals detected after B2E5-ADC treatment
(A) Representative images of ELuc-GIC brain tumor sections, ELuc-E6 (left graphs) and ELuc-E16 (right graphs), which were immunostained for Casp3 (red) and human

mitochondria (green). (B) Quantitative data of (A). All nuclei were labeled with Hoechst33342 (blue). Error bar indicates ±SD. Statistical significance was determined by the *t*-test. *** $p<0.001$, ****$p<0.0001$. Scale bar: 50 μm.

Since I used nude mice, which retain an active macrophage innate immunity, as brain tumor models, I performed immunostaining for F4/80, a marker for microglia and macrophage, on serial sections. I found that many F4/80+ cells infiltrated the brains injected with B2E5-ADC (Figure 21A). The percentage of F4/80+ cells in ELuc-E6 and ELuc-E16 brain tumors injected with B2E5-ADC was 11.8 ± 1.6% and 7.8 ± 1.9% respectively, whereas no F4/80+ cells were detected in the tumors injected with IgG, B2E5 or IgG-ADC, except that 0.1 ± 0.1% F4/80+ cells were detected in ELuc-E6 brain tumors injected with IgG-ADC (Figure 21B). Collectively, these findings establish B2E5 as a novel therapeutic agent for targeting GICs in GBM.

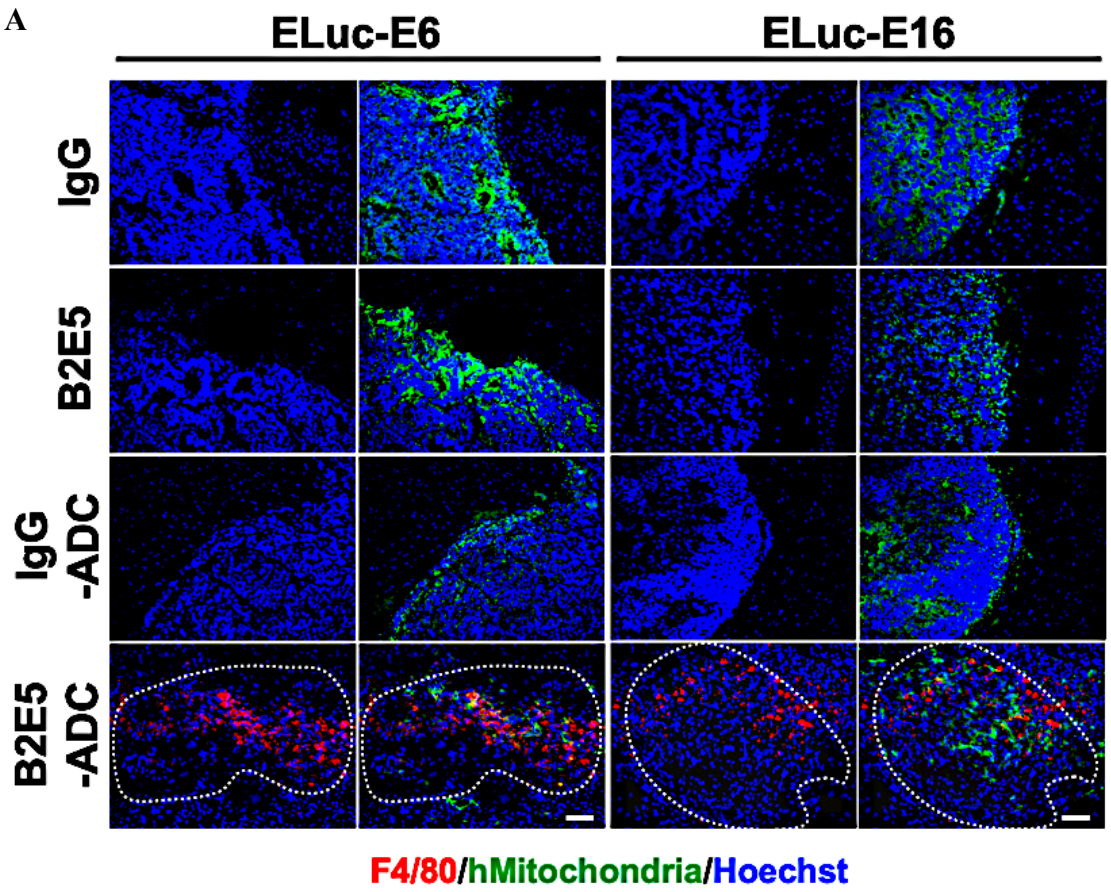

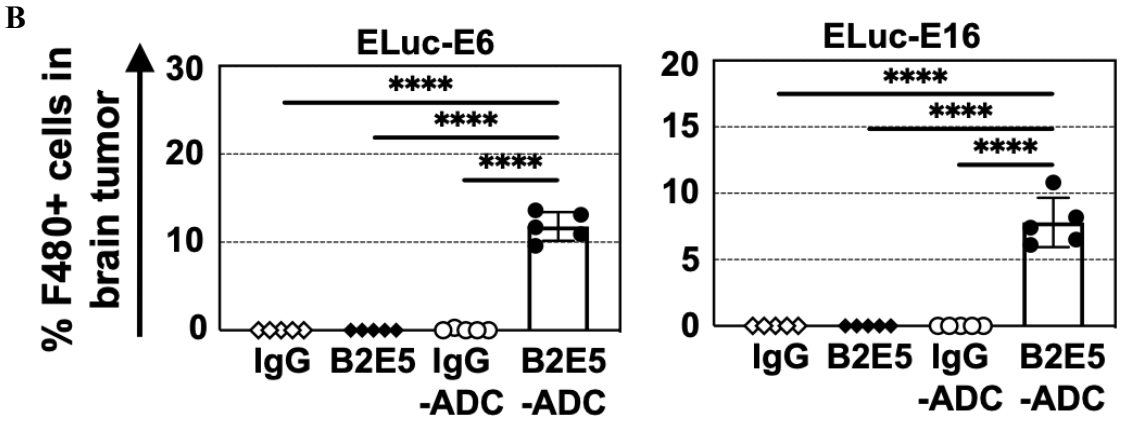

Figure 21: Macrophage aggregation after B2E5-ADC treatment

(A). Representative images of ELuc-GIC brain tumor sections, ELuc-E6 (left graphs) and ELuc-E16 (right graphs), which were immunostained for F4/80, a marker of microglia/macrophage (red), and human mitochondria (green). White dot lines showed hemosiderin deposit area. (lowest photographs). (B) Quantitative data of (A). All nuclei were labeled with Hoechst33342 (blue). Error bar indicates ±SD. Statistical significance was determined by the *t*-test. *** $p<0.001$, **** $p<0.0001$. Scale bar: 50 μm.

Discussion

Recent research has indicated that either ADCC or CDC might not be sufficiently efficacious in eradicating cancer *in vivo*. Firstly, it is a widely recognized fact that NK cells and cytotoxic T cells, which serve as the principal effector cells for ADCC and CDC respectively, express immune checkpoint factors like PD1 and NKG2A. Concurrently, cancer cells express ligands that have an affinity for these factors, thereby effectively neutralizing the anti-tumor activities of these effector cells (Wu et al, 2022). Secondly, research has demonstrated that hypoxia within the tumor microenvironment can directly impede NK cell activation by disrupting the MAPK signaling pathway and can also indirectly facilitate the recruitment of immunosuppressive cells, such as tumor-associated macrophages and regulatory T cells (Di Vito et al, 2019). Thirdly, it has been ascertained that hypoxia can enhance autophagic flux in cancer cells, hastening the degradation of granzyme B (Tong et al, 2022). Lastly, investigations have uncovered that cancer cells exhibit elevated levels of pro-survival BCL2 family proteins while simultaneously reducing the levels of pro-apoptotic proteins, which bolsters their resistance to cell death (Kaloni et al, 2023). Collectively, these research findings strongly suggest that the cytotoxicity of ADCC or CDC is restricted *in vivo*. In contrast, ADCs possess the unique capacity to directly target cancer cells and transport cytolysis agents, remaining unaffected by the cellular context or microenvironment of the target cells. ADC technology has also witnessed significant progress with the emergence of new cytotoxic agents, linkers, and artificial amino acids (Yang et al, 2023). Moreover, we can evaluate the anti-tumor activity of ADCs using tumor-bearing mice and assess their toxicity *in vivo*. Consequently, ADCs emerge as one of the most propitious alternatives for the development of novel anti-cancer pharmaceuticals. Based on these information, our B2E5-ADC could be a promising anti-GBM therapeutic medicine.

One of the challenges in the treatment of brain tumors is the delivery of therapeutic agents, including ADC, into the brain parenchyma across the BBB. Even though the tumor blood vessels formed by cancer cells are usually compromised, this still poses a major obstacle. Another essential factor is ensuring the delivery of a sufficient and high concentration of B2E5-ADC to effectively eradicate GICs in the brain. Taking these factors into consideration, I examined three different administration methods, intravenously, intrathecally and intracranially, and ultimately determined intracranial injection as the most effective method. However, due to the highly invasive nature of intracranial injection, it becomes extremely difficult to administer the ADC multiple

times. Therefore, it is crucial to either improve the administration methods for delivering B2E5-ADC or modify the ADC to use smaller antibody-based molecules, such as Fab-ADC and scFv-ADC, which can more easily traverse the BBB.

In this study, I found that although B2E5-ADC prolonged the lifespan of GIC-bearing mice, it couldn't completely cure the mice (all the mice died successively 60 days after tumor transplantation). There might be two reasons for this phenomenon. Firstly, the GIC tumors in the brain were not completely eliminated. Therefore, the tumors recurred after the B2E5-ADC administration was stopped, which led to the death of the mice. In response to this situation, it is necessary for us to either increase the concentration of B2E5-ADC or the frequency of drug administration to completely eliminate GIC. Secondly, it might be related to the severe damage to brain tissue caused by GBM and the inability to repair it in a timely manner. Brain tumors can lead to a variety of severe consequences such as neurological dysfunction, cognitive decline, epilepsy, increased intracranial pressure and related complications. In response to these phenomena, we still need to explore other treatment strategies, such as combined administration with drugs that can effectively accelerate brain damage repair.

I observed hemosiderin deposition in the brain that had been injected with B2E5-ADC, whereas no such deposition was observed in the brains injected with either IgG, B2E5, or IgG-ADC. This finding implies that the hemosiderin deposits likely originated from dead GBM cells (GICs), given that previous studies have demonstrated that GBM cells overexpress transferrin receptor and consequently accumulate iron within the cells. (Recht et al, 1990; Voth et al, 2015). Another possible explanation is that microglia or macrophages scavenged apoptotic GICs, which subsequently led to the formation of hemosiderin deposits. In either of these two scenarios, the occurrence of hemosiderin deposits presumably serves as an indicator or a characteristic feature of the elimination of GICs mediated by B2E5-ADC.

In the IgG-ADC administrated GIC tumor brains, a small amount of Cap3 signal was found, probably due to unstable linker breakage and toxic drug release. Optimization of ADCs is needed to cut normal tissue side effects. Otherwise, ADC administration may cause side effects like weakened immunity from reduced white blood cells, gastrointestinal issues, and hepatotoxicity. We still need more exploration on B2E5-ADC side effects.

We demonstrated that the intracranial injection of B2E5-ADC was highly effective in impeding brain tumorigenesis in the E6 and E16 models. For clinical translation and application, it will be necessary in the future to conduct further evaluations regarding the efficacy of B2E5-ADC in other well-established brain tumor models.

Conclusion

1. EVA1 is expressed in many types of gliomas and other malignant tumors. Glioma patients with elevated EVA1 mRNA levels have worse prognosis than that of other patients.
2. We have successfully obtained the anti-EVA1 antibody, B2E5, with high affinity for EVA1. B2E5 antibody exhibited strong ADCC and CDC activities against cells that express EVA1.
3. Considering Eva1 is a cell-surface protein and B2E5 can be internalized into GICs, we investigated the potential of B2E5 as a therapeutic antibody for GBM.
4. B2E5 recognized only human EVA1 but not mouse Eva1, its epitope is 72nd proline residue in EVA1.
5. B2E5-ADC killed ELuc-GIC *in vitro*. Moreover, intracranial administration of B2E5-ADC inhibited tumorigenesis in the brain. B2E5-ADC-injected tumor-bearing brains showed significant decreased tumor area and lost GBM pathological features.
6. I observed accumulated F4/80+ cells and Casp3 signals around the hemosiderin deposition in the brain injected with B2E5-ADC, which might suggest that infiltrating microglia/macrophages scavenged apoptotic GICs and contribute to the formation of hemosiderin deposition.
7. I tested three administration methods (intravenously, intrathecally, intracranially) and found intracranial injection most effective but hard for multiple ADC administrations due to its invasiveness.
8. In this study, B2E5-ADC was found to extend the lifespan of mice bearing GIC tumors.
9. Given the remarkable anti-tumor efficacy of B2E5-ADC, we could consider exploring humanized B2E5-ADC drugs to treat GBM patients. Likewise, humanized B2E5-ADC holds promise for treating other malignancies with high EVA1 expression.

Acknowledgement

We thank to Yoshikazu Sukenaga, Tokio Yamaguchi, Shigemi Yoshida, Atsushi Homma and Shigehiko Yamaguchi for their general support to this work. We also thank to Dr. Steve M. Hedrick for 2B4 cells, Dr. Yasuhito Onodera for ELuc cDNA, Yuri Tomabechi and Dr. Tomomi Kimura-Someya for antigen purification, Tomomi Uchikubo-Kamo for B2E5 cloning, Dr. Noboru Ohsawa for plasmid preparation, and Dr. Shenshen Dou for the MTT assay and mouse experiment.

Disclosure of Conflict of Interest

The author declares no conflict of interest.

References

Di Vito C, Mikulak J, Zaghi E, Pesce S, Marcenaro E and Mavilio D. (2019) NK cells to cure cancer. Semin Immunol. 41, 101272.

Guttinger M, Sutti F, Panigada M, Porcellini S, Merati B, Mariani M, Teesalu T, Consalez GG and Grassi F. (1998) Epithelial V-like antigen (EVA), a novel member of the immunoglobulin superfamily, expressed in embryonic epithelia with a potential role as homotypic adhesion molecule in thymus histogenesis. J Cell Biol. 141, 1061-1071.

Hide T, Takezaki T, Nakatani Y, Nakamura H, Kuratsu J and Kondo T. (2009) Sox11 prevents tumorigenesis of glioma-initiating cells by inducing neuronal differentiation. Cancer Res. 69, 7953-7959.

Hide T, Takezaki T, Nakatani Y, Nakamura H, Kuratsu J and Kondo T. (2011) Combination of a ptgs2 inhibitor and an epidermal growth factor receptor-signaling inhibitor prevents tumorigenesis of oligodendrocyte lineage-derived glioma-initiating cells. Stem Cells. 29, 590-599.

Kaloni D, Diepstraten ST, Strasser A and Kelly GL. (2023) BCL-2 protein family: attractive targets for cancer therapy. Apoptosis. 28, 20-38.

Kondo T. (2006) Brain cancer stem-like cells. Eur J Cancer. 42, 1237-1242.

Ni Q, Chen Z, Zheng Q, Xie D, Li JJ, Cheng S and Ma X. (2020) Epithelial V-like antigen 1 promotes hepatocellular carcinoma growth and metastasis via the ERBB-PI3K-AKT pathway. Cancer Sci. 111, 1500-1513.

Ohtsu N, Nakatani Y, Yamashita D, Ohue S, Ohnishi T and Kondo T. (2016) Eva1 Maintains the Stem-like Character of Glioblastoma-Initiating Cells by Activating the Noncanonical NF-κB Signaling Pathway. Cancer Res. 76, 171-181.

Powell MS and Hogarth PM. Fc receptors. (2008) Adv Exp Med Biol. 640, 22-34.

Recht L, Torres CO, Smith TW, Raso V and Griffin TW. (1990) Transferrin receptor

in normal and neoplastic brain tissue: implications for brain-tumor immunotherapy. J Neurosurg. 72, 941-945.

Roger Stupp, Warren P. Mason, Martin J. van den Bent, Michael Weller, Barbara Fisher, Martin J.B. Taphoorn, Karl Belanger, Alba A. Brandes, Christine Marosi, Ulrich Bogdahn, et al (2005) Radiotherapy plus Concomitant and Adjuvant Temozolomide for Glioblastoma. N Engl J Med. 2005;352(10):987–996.

Singh SK, Clarke ID, Hide T and Dirks PB. (2004) Cancer stem cells in nervous system tumors. Oncogene. 23, 7267-7273.

Stupp R, Hegi ME, Mason WP, van den Bent MJ, Taphoorn MJ, Janzer RC, Ludwin SK, Allgeier A, Fisher B, Belanger K, et al (2009) Effects of radiotherapy with concomitant and adjuvant temozolomide versus radiotherapy alone on survival in glioblastoma in a randomised phase III study: 5-year analysis of the EORTC-NCIC trial. Lancet Oncol. 10, 459–466.

Takezaki T, Hide T, Takanaga H, Nakamura H, Kuratsu J and Kondo T. (2011) Essential role of the Hedgehog signaling pathway in human glioma-initiating cells. Cancer Sci. 102, 1306-1312.

Tong L, Jiménez-Cortegana C, Tay AHM, Wickström S, Galluzzi L and Lundqvist A. (2022) NK cells and solid tumors: therapeutic potential and persisting obstacles. Mol Cancer. 21, 206.

Vescovi AL, Galli R and Reynolds BA. (2006) Brain tumour stem cells. Nat Rev Cancer. 6, 225-236.

Voth B, Nagasawa DT, Pelargos PE, Chung LK, Ung N, Gopen Q, Tenn S, Kamei DT and Yang I. (2015) Transferrin receptors and glioblastoma multiforme: Current findings and potential for treatment. J Clin Neurosci. 22, 1071-1076.

Wu C, Qin C, Long W, Wang X, Xiao K and Liu Q. (2022) Tumor antigens and immune subtypes of glioblastoma: the fundamentals of mRNA vaccine and individualized immunotherapy development. J Big Data. 9, 92.

Yamashita D, Kondo T, Ohue S, Takahashi H, Ishikawa M, Matoba R, Suehiro S, Kohno S, Harada H, Tanaka J, et al (2015) miR340 suppresses the stem-like cell function of glioma-initiating cells by targeting tissue plasminogen activator. Cancer Res. 75, 1123-1133.

Yang Y, Wang S, Ma P, Jiang Y, Cheng K, Yu Y, Jiang N, Miao H, Tang Q, Liu F, et al (2023) Drug conjugate-based anticancer therapy - Current status and perspectives. Cancer Lett. 552, 215969.